DISTINGUISHING REACHES IN A TROPICAL HEADWATER STREAM, COSTA RICA: UTILIZING MORPHOLOGY, INSTREAM WOOD, AND TERRESTRIAL LASER SCANNING IN HYDRAULIC CHARACTERIZATION

by

Peyton Everett Lisenby

Bachelor of Science, 2010
Sam Houston State University
Huntsville, Texas

Submitted to the Graduate Faculty of the
College of Science and Engineering
Texas Christian University
in partial fulfillment of the requirements
for the degree of

Masters of Science

May 2013

DISTINGUISHING REACHES IN A TROPICAL HEADWATER STREAM, COSTA RICA: UTILIZING MORPHOLOGY, INSTREAM WOOD, AND TERRESTRIAL LASER SCANNING IN HYDRAULIC CHARACTERIZATION

by

Peyton Everett Lisenby

Thesis approved:

Major Professor

For the College of Science and Engineering

ACKNOWLEDGEMENTS

I am endlessly grateful to my Mother and Father for their continuous support through every endeavor I have chosen to take on.

Special thanks goes to my thesis advisor, Michael Slattery, for allowing me to mold this project as I developed new understandings and for providing just the right amount of guidance (and funds) to make it a personally rewarding experience. Thanks to Thad Wasklewicz for his technical prowess, for playing an integral role in field surveys and critical reviews, and for indulging evening phone calls from the GIS laboratory. Thanks to John Holbrook for providing insight on the current state of hydraulic variables and coefficients and for being an excellent fluvial reference.

I sincerely appreciate the support in the field given by Stephanie Sunico, her daughter, Erica, Katie Reavis, and Gustavo Orozco. I would like to especially thank Stephanie for guiding me through the finer details of the School, for being a friend (and sometimes therapist), and for her constant encouragement. Thanks to Tamie Morgan for her longsuffering during my time in the GIS laboratory.

I would like to thank the Rocky Mountain Research Institute and ESSA Technologies, particularly Jim McKean and Nick Ochiski, for their help in troubleshooting the RBT.

I extend a special thanks to Chris Baldwin, Brian Cooper and Joe Hill at Sam Houston State University for their primary guidance in the field of Geology and scientific thinking.

This thesis is dedicated to Alejandra of FedEx International and “El Gordo Criminal” of Tical Trading Co. in San José, Costa Rica.

TABLE OF CONTENTS

LIST OF FIGURES

LIST OF TABLES

1. Introduction

Headwater streams (HWS) represent the foremost integration of climatic, tectonic, lithologic and biologic variables operating within a basin. HWS are often labeled "complex" or "high energy" because they display dramatic ranges in flow regime, channel morphology, and biodiversity. Visually, this characterization is easy to accept because few other geomorphic systems can harbor such a broad yet pronounced array of dynamic spatiotemporal features. Research of headwater system processes is commonly partitioned in the field, segregated in a flume, or simulated in a model to explain singular, distinct phenomena. This process-specific approach has certainly been useful when developing distinct models of bedload transport, step-pool stability, flow resistance prediction, and instream wood dynamics (Wilcox and Wohl, 2006; Yager et al., 2007; Nelson and Seminara, 2011; Curran, 2012). Multi-faceted approaches are required to address the inherent and complex interconnectivity associated with fluvial systems. This ensures methods and theories developed from centralized studies do not become exclusive from environmentally related processes (Nakamura et al., 2000; Dollar, 2002; Dollar et al., 2007).

Tropical HWS are leading examples of integrative geo-ecosystems that mandate more comprehensive research approaches. Climatic and biotic accelerated weathering, increased riparian bio-productivity, and seasonally flashy flow regimes only exacerbate the complex linkages already seen in temperate systems (Caine and Mool, 1981; Wohl, 2005; Pike et al., 2010). Further complication arises from their

remote locations and topographically challenging field sites. Aside from low accessibility, many of these streams are unmonitored, making it impossible to relate a flow regime record to observed channel change. The physical state of channel features is the most useful tool when characterizing ungauged streams, and makes accurate and precise spatial surveys the crucial component of investigation. Though tropical HWS systems are understudied in the literature, they provide great opportunities to observe impressive morphometric adjustments through a range of spatial and temporal scales.

This study presents a novel methodology for identifying, surveying, and modeling complex, tropical HWS reaches using channel morphology/wood distribution, orthographic terrestrial laser scanning (TLS), and 1-D hydraulics. 1-D modeling demonstrates the evolution of boundary shear stress and mean stream power through two reaches in an ungauged, tropical, montane HWS in Costa Rica. This foundational understanding supports continued multi-faceted research in tropical basins, and shows the evolution of TLS from an experimental geomorphological tool to one that is applicable and robust in challenging, tropical field sites.

2. Background

2.1. Channel Morphology and Instream Wood

A visual morphology classification system is a useful, readily available means of classifying reaches and channel segments in HWS. Montgomery and Buffington's (1997) classification system is widely used in temperate basins, and Wohl and Merrit (2008) showed quantifiable distinctions exist between the visually identified morphology categories. Wooldridge and Hickin (2002) found visual identification to be a proficient method in distinguishing step-pools and cascades based on step-span and grain-size partitioning. In tropical HWS, significant variation in flow regime and bed grain size along with highly weathered, paralithic bedrock substrates can cause smaller-scaled morphologies to be non-existent or unrecognizable (Jackson and Sturm, 2002; Wohl, 2005). An established classification scheme is still useful, but it may need some augmentation to describe unique morphology assemblages. A stepped-bed classification, as proposed and described by Grant et al. (1990) and Comiti and Mao (2012), is appropriate for steep, tropical HWS. It describes a stepped profile formed through grain steps and bedrock scour that is punctuated by individual step-pools, step-pool sequences, and cascading grain arrangements (Figure 1, *right*). This organized variability gives the field observer a measure of latitude when describing the highly variable and visually chaotic morphology assemblages common in tropical HWS.

The linkage between flow hydraulics, sediment dynamics, and channel morphology is affected by the occurrence of instream wood in forested headwater basins. The relationship between instream wood and fluvial processes has been extensively described over a wide range of basin and time scales (Piégay and Gurnell, 1997; Brooks and Brierley, 2002; Gurnell et al., 2002). Research in temperate HWS has shown that piece dimensions, arrangement, decay rate, and availability compared with flow regime and transport capacity determines residence time and stability in the channel. For a single piece, or multiple "jammed" pieces, residence time dictates how long the piece(s) can influence sediment flux and support reach-scale morphologies (Fetherston et al., 1995; Abbe and Montgomery, 1996; Massong and Montgomery, 2000; Hyatt and Naiman, 2001; Abbe and Montgomery, 2003; Faustini and Jones, 2003; Wohl and Goode, 2008; Wohl and Jaeger, 2009; Jones et al., 2011; Wohl et al., 2011). Whether or not a wood piece or jam can remain stable in the channel determines if its distribution will dictate or reflect flow hydraulics. More recent work has investigated instream wood and sediment-morphology-hydraulics relationships in tropical basins (Cadol et al., 2009; Wohl et al., 2009; Cadol and Wohl, 2010; Cadol and Wohl, 2011; Wohl et al., 2012). Steep, tropical HWS are largely transport dominated due to high decay rates and seasonal high intensity/frequency storm events; therefore, instream wood distribution is reflective of flow regime. The pieces that are most responsive to flow hydraulics are not "attached" to the lateral margins of the channel, and they serve as first-order indicators of previous flow conditions.

2.2. High-Resolution Topographic Surveys and Hydraulic Models

Over the past decade terrestrial laser scanning (TLS) has become a more utilized method for surveying and analyzing fluvial topographic surface variability at ultra-high, sub-decimeter resolution (Heritage and Hetherington, 2007; Hodge et al., 2009a; Hattanji et al., 2012; Milan and Heritage, 2012; Rychkov et al., 2012; Smith et al., 2012). TLS data-point cloud applications extend beyond first-order physical measurements to quantify flow hydraulics, roughness, bed stability, sediment flux, and large-scale volumetric changes at the centimeter scale in fluvial and debris-flow systems. (Milan et al., 2007; Heritage and Milan, 2009; Hodge et al., 2009b; Wasklewicz and Hattanji, 2009; McCoy et al., 2010; Cánovas et al., 2011; Schürch et al., 2011; Staley et al., 2011; Yager et al., 2012). Surface sampling advancements made through TLS have instigated improvements in interpolative techniques designed to maximize the accuracy and precision of digital elevation models (DEMs) used in geomorphic and hydraulic modeling investigations (Lane et al., 2003; Chaplot et al., 2006; Erdogan, 2009; Heritage et al., 2009; Reuter et al., 2009; Yilmaz, 2009; Wheaton et al., 2010; Milan et al., 2011; Schwendel et al., 2012).

Two critical components of hydraulic models are constraints on initial flow conditions and the surface on which flow is to be modeled. In ungauged streams, palaeostage markers found in the channel and riparian zone can be used to define initial flow conditions; though, imprecise interpretation of these markers can introduce error (Wohl, 1995; Pike and Scantena, 2010; Cánovas et al., 2011). TLS is especially useful for digital surface generation since it can be implemented below

any forest canopy and within the channel boundaries. TLS captures topographic irregularity at a finer scale than airborne LiDAR; however, when scanning from a tripod, it doesn't reflect true planimetric geometries. Effort must be made in the field to correct this so that ultra-high resolution can be coupled with an orthographic perspective when generating inputs for hydraulic models.

The scale and complexity of the geomorphological process being investigated is terminally linked to the accuracy and density of data describing the topographic surface. Model selection should be based on how well the surface data can be utilized to maximize model effectiveness and prevent over-prediction (Aggett and Wilson, 2009). Improved DEM resolution will correspondingly advance predictive capacity only if the selected model is sensitive to the resolution of that surface (Horritt et al., 2006; Hengl and Evans, 2009). By combining ultra-high resolution DEMs and accurate interpretation of riparian stage indicators into a flow simulation, geomorphologists, engineers, and stream managers can relate flow hydraulics to any physically mappable channel element and generate hydraulic models that explain and/or predict fluvial processes in detail (Ferguson, 2003; Harrison and Keller; 2007; Cánovas et al., 2011; Yochum et al., 2012).

2.3. Study Site

The study stream (10° 15' 11.294" N, 84° 33' 19.564" W) is the primary drainage within a headwater basin of the Río San Lorencíto situated in the

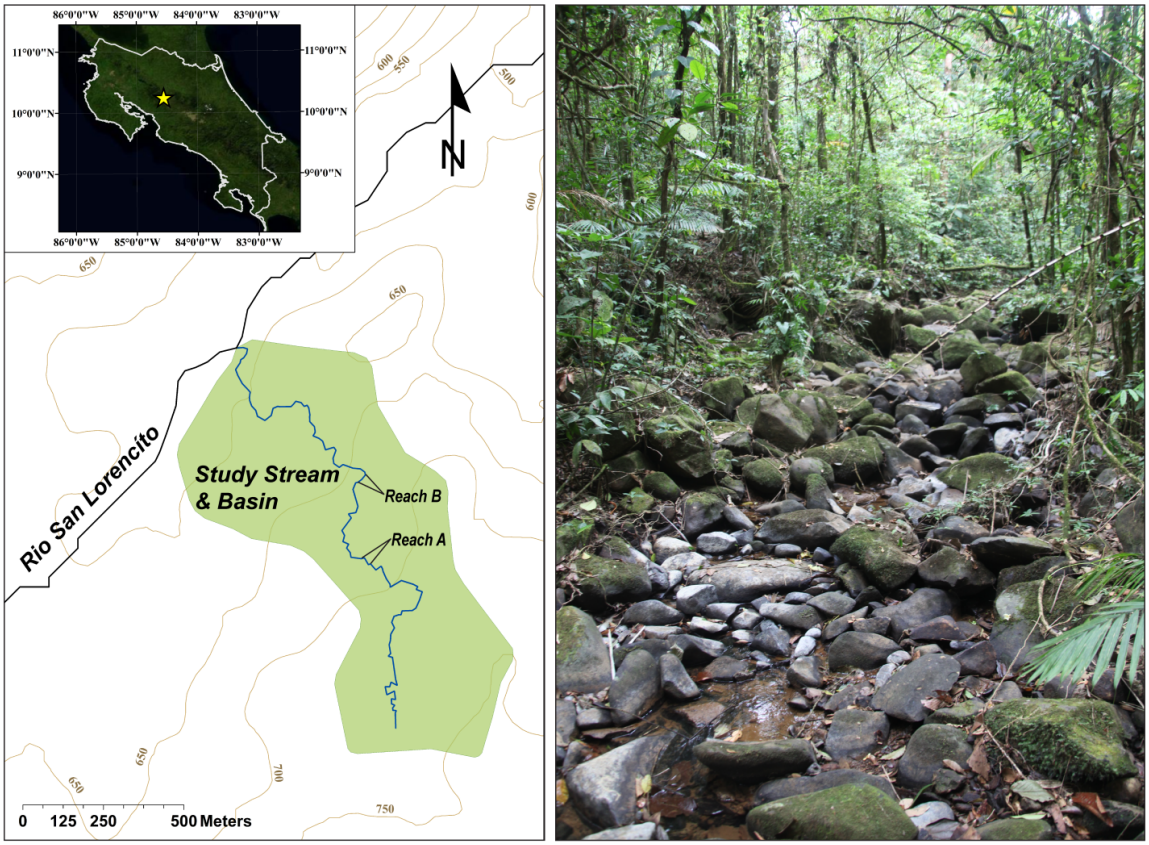

Figure 1. Field Location. *Left* – study stream and basin. *Right* – stepped-bed portion of the channel where channel width ≈ 5m; photo taken in February during the dry season.

Cordillera de Tilarán in North-central Costa Rica (Figure 1, *left*). The unnamed headwater stream is a steep channel (stream average gradient ~16%) draining ~0.7 km^2 of a tropical montane sub-cloud forest, an ecotone between the cloud forests and tropical lowlands of this region. The stream lies within the Texas Christian University Tropical Research Station; a 100-hectare property located at 600m asl to 800m asl and covered with cleared pasture and mixed pristine/secondary growth broadleaf forests (Ozenick, 2010). This area receives over 4000mm of rainfall annually, most of which falls in the wet season from June through September during intense, short duration, high frequency storms. Mean annual temperature for the region is 21° C, with an average range of 16° C annually (Maue and Springer, 2008).

The stream is generally characterized as a 2^{nd}-order, boulder-bed channel set into a saprolitic andesite substrate with steep confining valley walls of deep oxisol soils that frequently fail and slump, contributing fine-materials from the hillslopes to the channel. Stream flow competence during the wet season is capable of removing these slugs of fine sediment through the channel as is evident in a lack of non-vegetated bar deposits and lack of fine materials stored in pools. The channel is functionally disconnected from the hillslope in terms of coarse material. No evidence of debris flows or hyperconcentrated flows were uncovered during initial field reconnaissance.

The coarse materials in the channel and substrate are arranged into a stepped-bed form (Figure 1, *right*) with sequences of distinct and intermingled step/pools, cascades, meanders, and bifurcations around vegetation-stabilized mid-channel bars composed of finer sediments contributed from the riparian slope

failures. The stream originates in secondary growth forest and traverses ≈ 2000m toward primary forest exhibiting downstream trends of increasing riparian valley slope and tree diameter at breast height (DBH), maximum grain size, step heights, and bedrock incision.

The stream length shown in Figure 1 excludes the upper 200m of stream channel because it extends outside the boundaries of the research station. This outside section traverses a mostly deforested property and has two small impoundments. We believe that this cleared section contributes fine-grained (coarse sand-fine gravel) sediments to the upper portion of the mapped stream, which will be discussed later.

3. Methodology

3.1. Field Methods

Initial field reconnaissance was completed in February 2012, during the early dry season. Fieldwork was conducted at the end of the dry season, from May 16th through May 21st, 2012, so that the channel would have a minimal amount of water and be navigable by foot, and so precipitation would not interfere with any sensitive electronics in order to maximize uninterrupted scanning time.

3.1.1. Channel Morphology and Instream Wood Survey

The stream length contained within the research station boundaries was surveyed with a GPS (Trimble Geo XH 6000 mounted to a 15' telescopic beacon) to demarcate distinct morphological reaches where instream wood would be assessed. Points were recorded along the channel thalweg while morphologies and morphology transitions were visually identified (Wooldridge and Hickin, 2002). Populations of instream wood were segregated by morphology-reach. Five distinct reach morphologies were identified over the length of the stream (Table 1). Instream wood pieces were classified similar to Cadol et al. (2009), but with some modification (Figure 2). A bridge spans the channel, with each end resting on either bank. A ramp has one end resting on the channel bank and the other within the channel to include a piece with one end resting on the bank and the other resting on

Table 1
Descriptions of reach morphologies.

Morphology	Description
alluvial	*meandering, low gradient channel on an alluvial substrate*
bifurcated	*widened as compared to other reaches with one or two meander bends with the occurrence of vegetation stabilized mid-channel bars*
step-pool	*primarily multiple step-pool sequences of three to six ribs with the possible occurrence of intermittent, short cascades and/or individual step-pools*
straight stepped-bed	*primarily cascades with individual step-pools bound by bifurcated reaches*
meandering stepped-bed	*cascades with individual step-pools bound by step-pool and/or bifurcated reaches*

Figure 2. Designations of instream wood occurrence. A – bridge, B – ramp, C – unattached, D – Unattached-emplaced, E – Vine-entangled

a mid-channel bar. An unattached piece lies completely within the channel to include pieces resting completely on a mid-channel bar. An unattached-emplaced piece rests completely within the channel and is partially buried or incorporated into a "forced" morphology, as described by Montgomery and Buffington (1997). A vine-entangled piece is ensnared in riparian or mid-channel bar vines and is partially or completely suspended above the channel bed. Minimum size conditions for an individual piece to be included in the survey were a 10cm half-circumference (6.4cm diameter) and 1m length. This expands the number of assessable pieces for visibly wood-staved systems similar to Wohl and Goode (2008).

Any wood pieces that failed to meet our size conditions were excluded from the survey along with any living roots, rooted stumps (emplaced in the ground), vines, living trees rooted in or lying in the channel, and palm fronds. Since all wood volumes were calculated as approximate cylinders, we also excluded any piece that was deteriorated enough to where that approximation could not be made. Pieces with multiple branches were considered a single piece and the lengths of the branches, sized above the minimum conditions, were added to the main beam length. Wood load was calculated for each reach, by dividing reach wood volume by the reach length, and normalized to 100m channel lengths. Wood abundance was calculated by dividing the reach wood piece total by the reach length and also normalized to 100m. A 100m normalization factor was chosen due to the visual dearth of instream wood. The reach lengths were derived from the GPS survey and differently corrected using a base station in Managua, Nicaragua.

3.1.2. Reach Selection and Terrestrial Laser Scanning

Twenty-nine separate reaches were identified in the field based on observed morphology transitions. These reaches were classified according to the parameters shown in Table 1. Two bifurcated reaches, A and B (Figure 1, *left*), were selected for TLS surveying based on their sequence of morphological elements and observations of instream wood distribution. Each reach displayed a downstream progression from a step-pool or stepped-bed morphology to a widened meander bend with a vegetation-stabilized mid-channel bar (Figure 3). Special attention was given to unattached piece deposition. Studies conducted in tropical HWS at the La Selva Biological Station, Costa Rica demonstrate that instream wood distribution is primarily controlled by fluvial transport capacity (Cadol et al., 2009). Additionally, Wohl et al. (2009) found that high, wet season transport capacities fundamentally dictate wood load variation. Unattached instream wood pieces are the most responsive to fluvial transport capacity variation (Cadol and Wohl, 2010), and their distribution is used to accent the morphological complexity observed in the selected reaches. Field reconnaissance showed reaches A and B to contain higher instream wood abundance and loading, especially regarding unattached pieces, as compared to adjacent morphologies. This observational trend was consistent through the entire stream coarse. The widened channel, mid-channel bars and instream wood deposition indicate that these bifurcated reaches as areas preceded by high flow competence and transport capacity, and that they are influential in modulating flow kinetics.

Figure 3. Downstream morphology progression in reaches A (left) and B (right). *Top* – step-pool sequences at the uppermost portion of each reach. *Center* – meander bend immediately downstream of step-pools, looking upstream. *Bottom* – mid-channel bars, looking downstream in reach A and upstream in reach B. Field book for scale.

Terrestrial laser scanning surveys were conducted using a Leica HDS 7000. The HDS 7000 employs phase-based measurements of a continuous infrared laser pulse (1.5μm wavelength). The TLS instrument was suspended 2.3m above the ground surface, upside-down on a mobile aluminum frame resembling a swingset (Figure 4). This set-up permits a true, orthographic perspective of the channel, reflecting the most representative hydraulic geometry. The TLS unit is mounted on a 7.62cm (3" ID) sleeve fitted around the central beam, suspended from the center of the frame. The TLS swingset was placed in the channel where each leg firmly contacted the channel bottom. The frame is not required to be perpendicular to or parallel with the channel, nor did the central beam have to remain level. Only the necessary coverage area and leg support dictated the placement of the frame. The TLS unit control software was integrated with an iPad so that the scan could be initiated remotely. An individual scan took 6 minutes to complete and covered a maximum 360° x 320° field of view, generating a point cloud of approximately 15 million data points.

The point cloud generated from each scan must be spatially referenced. Multiple spatially-related TLS swingset scan positions are required for each reach to adequately cover their proportions and to accommodate the shadows created by boulders, instream wood, and mid-channel bars. Tripod mounted, 15cm planar targets were systematically positioned throughout the channel reach (Figure 4). The overlapping positions of these targets allow sectional scans to be linked in post-processing and related to a Cartesian coordinate system to create a continuous, spatial data surface. The targets also dictate the orientation of the x, y, z directions,

Figure 4. Terrestrial Laser Scanning (TLS) and target locations in reach A, looking downstream.

so it is imperative that the targets are level. Their locations were affixed by mounting the tripods directly atop expansion bolts inserted into large boulders and bedrock of the channel margins. Near-channel areas were minimally cleared so that the scanner would have a clear line-of-sight to the targets; however, all instream wood was left in place. Oblique, tripod mounted, scans were also used to augment surface coverage and to "right" the data. Since the TLS unit was suspended upside-down from the frame, the positive z direction is oriented down. Adding a supplementary oblique scan to a series of suspended scans supplies an upward positive Z direction to which all other scans can be linked. Reach A required 12 scanning positions, including one oblique scan. Reach B also required 12 scanning positions but without an oblique scan (reach B point clouds were "righted" in post-processing). All scans were conducted under low flow conditions during periods of no rain to ensure that there was no moisture interference in the air or on the reflective channel surfaces.

3.2. TLS Laboratory Methods (Post-Processing)

3.2.1. Point Cloud Registration and Error Assessment

Point cloud datasets were registered in Leica Geosystems Cyclone software v. 7.4. For reach A, all scans were registered together, using the target locations, with the oblique scan to generate a continuous, righted point cloud. For reach B, the 12

Table 2
Assessment of point cloud error measured at target locations across each reach.

Vector	Error Metric	Reach 2 Error (mm)	Reach 3 Error (mm)
X	SE	-0.03	0.02
	MAE	0.93	0.23
	RMSE	1.38	0.50
	σ	1.50	0.76
Y	SE	-0.01	0.08
	MAE	1.16	0.32
	RMSE	1.72	0.67
	σ	1.87	1.00
Z	SE	-0.04	0.02
	MAE	0.06	0.09
	RMSE	0.24	0.31
	σ	0.26	0.47

suspended scans were registered together with a text file of the target locations that reversed their "z" orientation to produce a continuous, righted point cloud. Error was assessed at the level of this raw, point cloud data to consider error in the x, y and z directions. Vertical errors (z) significantly influence DEM quality at lower gradients, while horizontal (x and y) errors are more significant at higher gradients (Wheaton et al., 2010). Systematic error, or mean error (SE), mean absolute error (MAE), root mean square error (RMSE), and the standard deviation (σ) of error are measured at control point locations (expansion bolts set in the channel substrate). The black and white planar targets placed here reflect data points during a scan. These points are used to assess error between scans. Sample populations are 165 and 102 points for reach A and B, respectively. Errors in x, y and z (Table 2) for each survey are based on the standard deviation of errors at the control points given:

$$\sigma = \sqrt{\frac{1}{N}\sum_{i=1}^{N}(\delta_t - \mu)^2} \qquad (1)$$

where N = the number of control points, δ_t = the error at control point t (in x, y, or z directions), and μ = the mean error at all control points (calculated individually for x, y and z directions).

3.2.2. Point Cloud Cleaning and Filtering

The reach point clouds captured the channel bed and riparian slopes. DEM interpolation requires a bare channel bed and slope surface. The dense rainforest vegetation on the slopes along with all channel and bar vegetation and instream wood were manually cleaned in Cyclone to prepare the point cloud surface for subsequent filtering. The positions of all instream wood were marked in Cartesian space prior to cleaning. The reach point clouds were partitioned into overlapping bed, bank, and bar sections and cleaned individually to maintain easily manageable file sizes. Vegetation on the riparian slope sections was "shaved" to within a few meters of the ground surface. After cleaning, the point cloud sections were exported to LasTools filtering software as .las files (Isenburg et al., 2006). For both reach point clouds, the sections were converted to .laz files and "tiled" into further paneled segments using LasTile. These tiled sections were then "thinned" to remove vegetation and spurious point data. For bed sections, the LasThin filter was run over a 1cm grid, keeping the highest point within each grid. For bank and bar sections, the tool was run over a 5cm grid, keeping the lowest point within each grid cell to assume that there is at least one true ground surface point within every 5cm square of each bank and bar section. Additionally, the bank and bar sections were further thinned using the LasDuplicate filter which kept the lower of two points with the same x, y coordinates. Lastly, the bank and bar section tiles were vegetation filtered using the LasGround tool to remove any vegetation points that persisted. This prevents a false ground surface composed of vegetation from being retained in the

point cloud data, but also produces a less dense point coverage on the slopes. Adjustments were made within the LasGround tool to balance the points removed versus retained. All section tiles were then reassembled and exported to ArcGIS as multipoint shapefiles. Mean surface data densities for bed and bank/bar portions of reach A were ≈ 6507 points/m^2 and ≈160 points/m^2, respectively, for a reach total of 2.75 million points. For reach B, mean data densities for bed and bank/bar portions were ≈ 6878 points/m^2 and 105 points/m^2, respectively, for a reach total of 5.74 million points.

3.2.3. DEM Interpolation

Each multipoint section was given a bounding polygon shapefile and stored as a terrain dataset in ArcMap 10.0 where the terrain could be viewed as a TIN surface. The terrain datasets were then converted to 2cm resolution raster DEMs using a single linear interpolation. The sections were interpolated for each reach and then mosaicked together; using the overlap given during the original partitioning in Cyclone, into continuous 2cm resolution reach raster surfaces (Figure 5). For the bed surfaces, the overlapping areas were averaged. When mosaicking the bed to the banks and bar sections, the bed cell values were retained.

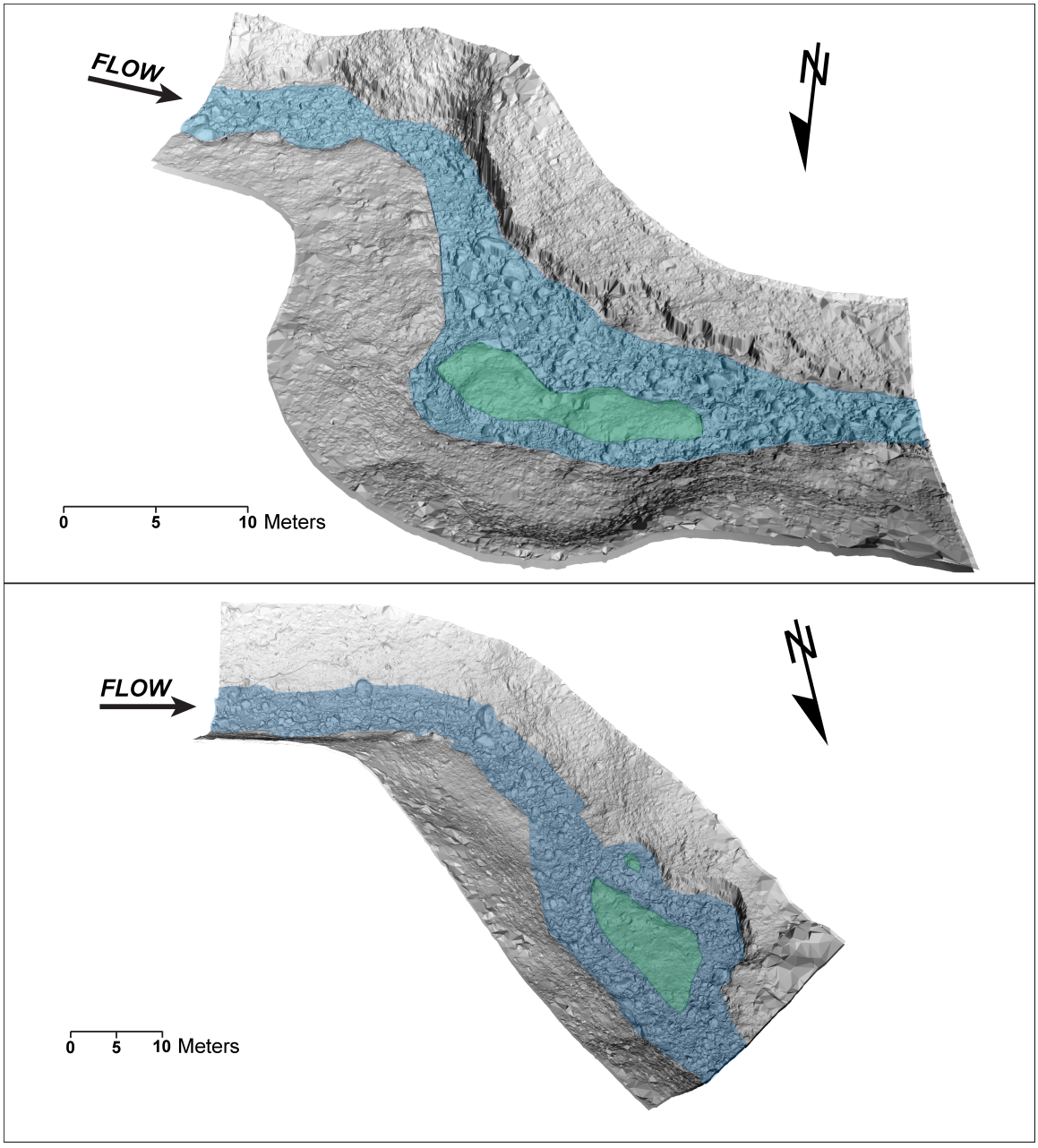

Figure 5. DEMs of reaches A (top) and B (bottom). Blue shaded area gives the extent of the boulder channel bed. Green shaded area gives the extent of mid-channel bars.

3.2.4. 1-D Hydraulic Modeling

The DEMs were digitally surveyed with cross-sections using the River Bathymetry Toolkit (RBT), a toolbar designed to work within ArcMap 10.0 (McKean et al., 2009). After detrending the longitudinal slope from each DEM, flow levels (flood heights) were delineated by simulating static water inundation of the detrended raster surface. This "fills" the DEM channel with water up to a user specified level and outputs a "bankfull" polygon depicting the extent of the flood boundary. Two flow levels were chosen based on flood height evidence seen in the field. Instream wood and boulders were seen deposited on and imbricated against the face of the mid-channel bars (Figure 2, bottom). This was used to represent the modeled high-flow level. A low-flow level was also selected so that flow would just bypass the secondary overflow channels, around the mid-channel bars, and remain in the channel thalweg. Water surface elevations between flow levels differed by 0.6m and 1m for reach A and B, respectively. Centerlines were manually drawn in ArcMap to approximate the longitudinal center of the channels represented by the bankfull polygons. Cross-sections were then measured every streamwise meter along the channel centerlines with individual channel-raster elevations recorded every 5cm across each cross-section. For reach A the low- and high-flow levels required 47 and 49 cross-sections, respectively, to cover their streamwise length. For reach B, the low- and high-flow levels required 76 and 73 cross-sections, respectively. For both flow levels of each reach, the RBT output a spreadsheet containing the raster cell elevations recorded at 5cm intervals along each cross-

section, so that a population of bed elevations would represent the extent of each individual cross-section across the channel, and a population of cross-sections would represent each flow-level for both reaches.

Elevation spreadsheet data for all cross-sections were exported to Excel where wetted perimeter (P), bankfull area (A), hydraulic radius (R), mean depth (d), and slope (S) were calculated manually for each individual cross-section. The RBT will calculate these values automatically in ArcMap while it measures the cross-sections; however, during troubleshooting of the toolkit, it was found that it did not always consider channel raster elevations on both sides of a water-surface-protruding boulder. Manually calculating hydraulic geometries in a spreadsheet ensured that all cross-sectionally measured elevations that fell beneath the simulated "bankfull" flow elevation were considered. Bed slope was calculated for each cross-section by considering the cross-sectional elevations 2m up and downstream; except for the low-flow condition in reach A, where slope calculations considered elevations 3m up and downstream. Formulae for P, A, R, d, and S can be found in the RBT workbook, available free online through the US Forest Service Rocky Mountain Research Station, Boise Laboratory. Additionally, the standard deviation of bed elevations (σ_z) for each cross-section was calculated using their respective populations of 5cm incremented elevation measurements. From these hydraulic geometries, for an individual cross-section, velocity (V) was calculated using:

$$V = \left(\frac{d}{\sigma_z}\right) u^* \ \text{(m/s)} \quad (2)$$

where $u^* = \sqrt{gdS}$, *shear velocity* and g = 9.81 m/s^2 (Yochum et al., 2012). Boundary shear stress (τ), and mean stream power (ω) were calculated using:

$$\tau = \gamma RS \ \text{(N/m}^2\text{)} \quad (3)$$

$$\omega = \gamma RSV \ \text{(W/m}^2\text{)} \quad (4)$$

where γ = 9810 N/m^3, the specific weight of water (Fonstad, 2003), so that

$$\omega = \tau V \ \text{(W/m}^2\text{)} \quad (5)$$

Values of τ and ω were assigned as attributes to each cross-section, for each flow level and reach, in a spreadsheet and joined to cross-section shapefiles and then overlain atop the reach DEMs in ArcMap.

Equations 2-5 (along with hydraulic geometry calculations) define a one-dimensional, analytical model used in conjunction with the ultra-high resolution DEMs and the RBT. Values of τ and ω are solutions calculated from these algebraic equations using direct recordings of raster surface values and represent depth-

averaged products for an individual cross-section. This analytical approach was selected because it incorporates only direct measurements of the topographic data. Therefore, these measurements are subject to only the primary spatial errors quantified in the point cloud and preserved in the DEMs, and error is not amplified because it is not propagated through computational steps.

4. Results

4.1. Morphology and Instream Wood Distribution

Instream wood across all morphologies totaled 385 pieces for ≈ 110 m^3 of wood volume yielding a total instream wood abundance of 18.9 pieces/100m and a loading of 5.4 m^3/100m (Table 3). Unattached pieces account for nearly 63% of total abundance and 31% of total volume. Despite being less than half as numerous, ramps made up a larger portion of the total volume (59%) as they tended to be larger than unattached pieces in the lower course of the stream profile. Bifurcated reaches contain ≈ 47% and ≈ 57% of the total stream wood abundance and volume, respectively, and ≈ 55% of the abundance and ≈ 63% of the volume of unattached instream wood occur in bifurcated reaches (Table 4). Bifurcated reaches are present throughout the longitudinal course of the stream, and they become progressively longer in the lower half which spatially corresponds with unattached pieces becoming larger and more numerous. In general, both total and unattached wood abundance and loading increase with downstream distance (Figure 6), along with individual piece size. Straight and meandering stepped-bed morphologies are restricted to the upper half of the stream profile, along with the single alluvial reach, which limits their effectiveness for storing instream wood beyond immediate local recruitment. Bridge and ramp pieces become larger downstream but not progressively more numerous, and unattached-emplaced and vine-entangled pieces are not common enough across any morphology to display a downstream trend.

Table 3

Instream wood abundance and loading for all morphologies. Abundance and loading values for total instream wood and unattached pieces correspond with the symbology of Figure 6.

Reach ID	Morphology	Reach Length	Bridge		Ramp		Unattached		Unattached-Emplaced		Vine-Entangled		Total			
			Abun.	Load.	Abun.	Load.	Abun.	Load.	Abun.	Load.	Abun.	Load.	#	Vol.	Abun.	Load.
		(m)	(#/100m)	(m^3/100m)	(#/100m)	(m^3/100m)	(#/100m)	(m^3/100m)	(#/100m)	(m^3/100m)	(#/100m)	(m^3/100m)		(m^3)	(#/100m)	(m^3/100m)
1	aluvial	186.93	4.28	0.95	8.02	0.20	4.81	0.09	1.60	0.0086	1.07	0.08	37	2.63	19.79	1.41
2	straight stepped-bed	68.78	---	---	---	---	---	---	---	---	---	---	0	---	---	---
3	bifurcated	24.10	4.15	0.08	---	---	4.15	0.10	---	---	4.15	0.05	3	0.06	12.45	0.23
4	straight stepped-bed	27.63	---	---	---	---	---	---	---	---	---	---	0	---	---	---
5	bifurcated	33.13	6.04	0.36	12.07	1.47	3.02	1.97	---	---	---	---	7	1.26	21.13	3.80
6	straight stepped-bed	27.35	---	---	---	---	10.97	0.19	---	---	---	---	3	0.05	10.97	0.19
7	bifurcated	18.25	---	---	---	---	5.48	0.30	---	---	---	---	1	0.05	5.48	0.30
8	step-pool	30.54	---	---	---	---	---	---	---	---	---	---	0	---	---	---
9	bifurcated	50.90	---	---	---	---	3.93	0.06	---	---	---	---	2	0.03	3.93	0.06
10	meandering stepped-bed	73.47	1.36	0.05	9.53	0.17	9.53	0.10	---	---	---	---	15	0.23	20.42	0.31
11	step-pool	84.39	1.18	0.11	7.11	0.63	1.18	0.01	---	---	1.18	0.04	9	0.68	10.66	0.80
12	bifurcated	41.78	---	---	---	---	---	---	---	---	2.39	0.03	1	0.01	2.39	0.03
13	straight stepped-bed	20.90	4.78	0.31	4.78	0.29	14.35	0.31	---	---	---	---	5	0.19	23.92	0.91
14	bifurcated	59.24	---	---	5.06	0.86	6.75	0.65	1.69	0.0285	1.69	0.62	9	1.29	15.19	2.18
15	step-pool	27.18	---	---	7.36	1.75	3.68	1.99	---	---	---	---	3	1.02	11.04	3.74
16	bifurcated	35.49	---	---	5.64	0.36	22.54	2.28	---	---	---	---	10	0.94	28.18	2.64
17	meandering stepped-bed	200.98	---	---	3.98	0.26	10.95	0.45	0.50	0.0025	2.99	0.21	37	1.89	18.41	0.94
18	step-pool	116.20	0.86	0.27	4.30	0.99	1.72	0.12	---	---	---	---	8	1.61	6.88	1.38
19	bifurcated	63.07	---	---	9.51	1.40	19.03	1.71	---	---	1.59	0.04	19	1.99	30.12	3.15
20	bifurcated	51.15	1.95	5.05	---	---	31.28	10.49	---	---	1.95	0.49	18	8.20	35.19	16.03
21	step-pool	154.24	0.65	0.29	3.24	1.02	9.72	1.11	---	---	0.65	0.06	22	3.83	14.26	2.48
22	bifurcated	76.23	---	---	6.56	7.07	35.42	4.99	---	---	---	---	32	9.20	41.98	12.06
23	step/pool	55.13	---	---	14.51	5.78	7.26	1.39	---	---	---	---	12	3.95	21.77	7.17
24	bifurcated	37.52	---	---	18.66	2.34	31.99	3.58	---	---	---	---	19	2.22	50.65	5.92
25	step-pool	52.60	---	---	5.70	13.24	15.21	6.49	---	---	---	---	11	10.38	20.91	19.72
26	bifurcated	107.81	0.93	3.66	4.64	21.19	25.97	5.05	---	---	---	---	34	32.24	31.54	29.91
27	step-pool	175.98	---	---	2.27	8.43	14.77	2.57	0.57	0.0032	---	---	31	19.45	17.62	11.05
28	bifurcated	61.81	---	---	12.94	5.76	32.35	4.18	---	---	---	---	28	6.14	45.30	9.94
29	step-pool	73.93	---	---	---	---	12.17	0.61	---	---	---	---	9	0.45	12.17	0.61
	Total	2036.71	0.88	0.46	5.11	3.17	11.88	1.69	0.29	0.0001	0.74	0.07	385	109.986	18.90	5.40

Table 4
Abundance and loading percentages according to occurrence type and morphology.

Morphology	Bridge		Ramp		Unattached		Unattached-Emplaced		Vine-Entangled		Total	
	# Pieces (%)	Vol. (%)	# Pieces (%)	Vol. (%)	# Pieces (%)	Vol. (%)	# Pieces (%)	Vol. (%)	# Pieces (%)	Vol. (%)	# Pieces (%)	Vol. (%)
alluvial	44.44	18.88	14.42	0.58	3.72	0.50	50.00	50.89	13.33	11.31	9.61	2.39
straight stepped-bed	5.56	0.69	0.96	0.09	2.48	0.34	0.00	0.00	0.00	0.00	2.08	0.22
bifurcated	27.78	70.98	38.46	53.78	54.55	62.72	16.67	7.23	33.33	49.02	47.53	57.85
step-pool	16.67	9.10	31.73	44.54	27.27	33.58	16.67	29.21	13.33	9.26	27.27	37.60
meandering stepped-bed	5.56	0.35	14.42	1.01	11.98	2.86	16.67	12.67	40.00	30.41	13.51	1.93
Total (%)	4.68	8.54	27.01	58.64	62.86	31.29	1.56	0.29	3.90	1.24	100.00	100.00

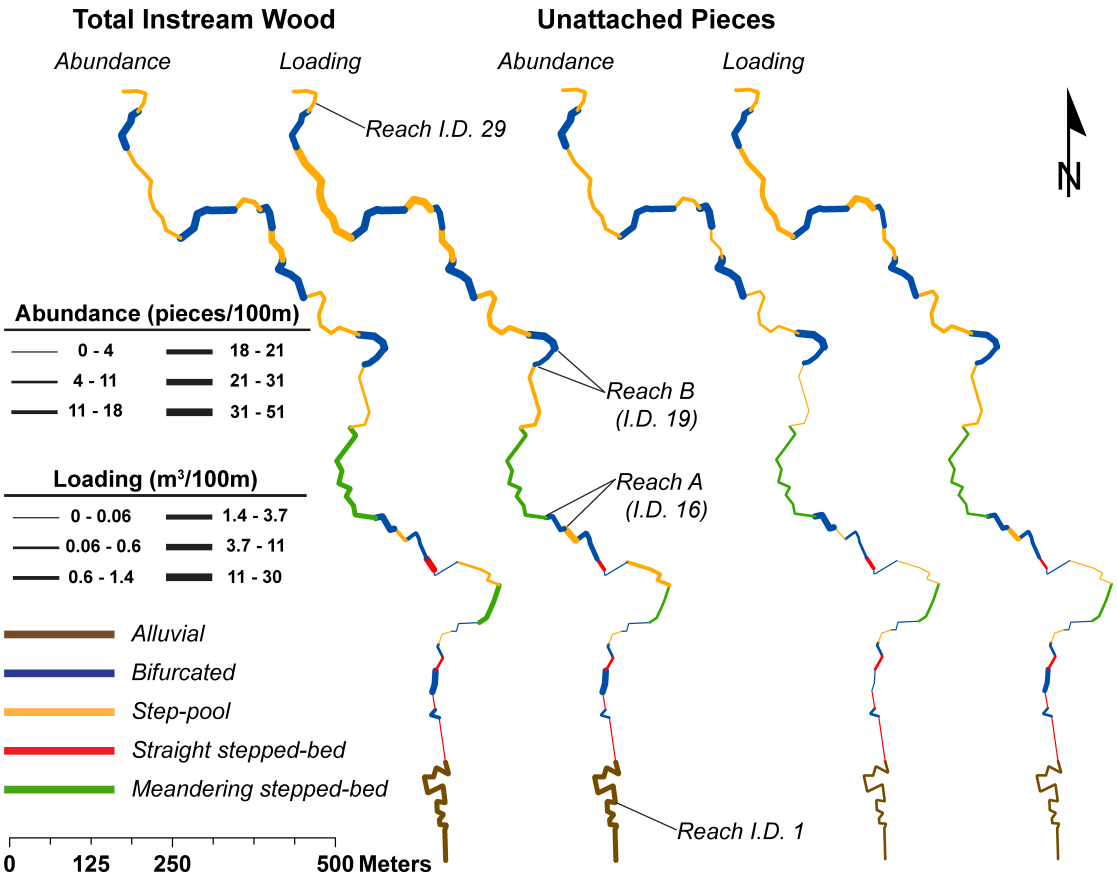

Figure 6. Total instream and unattached piece abundance and loading symbolized by quantile classification. See Table 3 for morphology-specific values of abundance and loading. Reach B transitions to another bifurcated reach through a short stepped-bed segment that is not demarcated.

Reaches A and B are located in the central third of the stream course, with reach B positioned ≈ 300m downstream from reach A (Figure 6).

4.2. Morphological Trends in Shear Stress and Stream Power

Figures 7-10 detail the down-reach variation in boundary shear stress (τ) and mean stream power (ω). Profiles of τ and ω mimic one another in reach A for both flow conditions, so shear stress state is indicative of energy expenditure (Figures 7, 8). The minor differences between them are attributable to V consideration in ω calculations. Reach A begins with flow entering a pool and then progressing over a step (Figures 7, 8, cross-sections 0-8). This "pool-step" profile is hydraulically recognizable at the high flow condition as τ and ω decrease through the pool and peak over the step. The low flow condition does not generate enough τ or ω to clearly resolve this morphology. Thalweg relief in reach A is not locally significant enough to see the correlation of step slope with either hydraulic variable. τ and ω increase through the first meander bend (Figures 7, 8, top, cross-sections 7-13), where the highest values of ω occur under low flow. This is not seen at high flow, spatially corresponding with lateral margin inundation (Figures 7, 8, bottom, cross-sections 7-20). Another set of elevated τ and ω values occur around the mid-channel bar (low flow, cross-sections 30-40) and over the mid-channel bar (high-flow, cross-sections 29-40). These patterns are interpreted to correspond with local S variation on and around the bar since S calculations are sensitive to bed surface variation over short (2m-3m) distances. Past the bar, the channel transitions into a

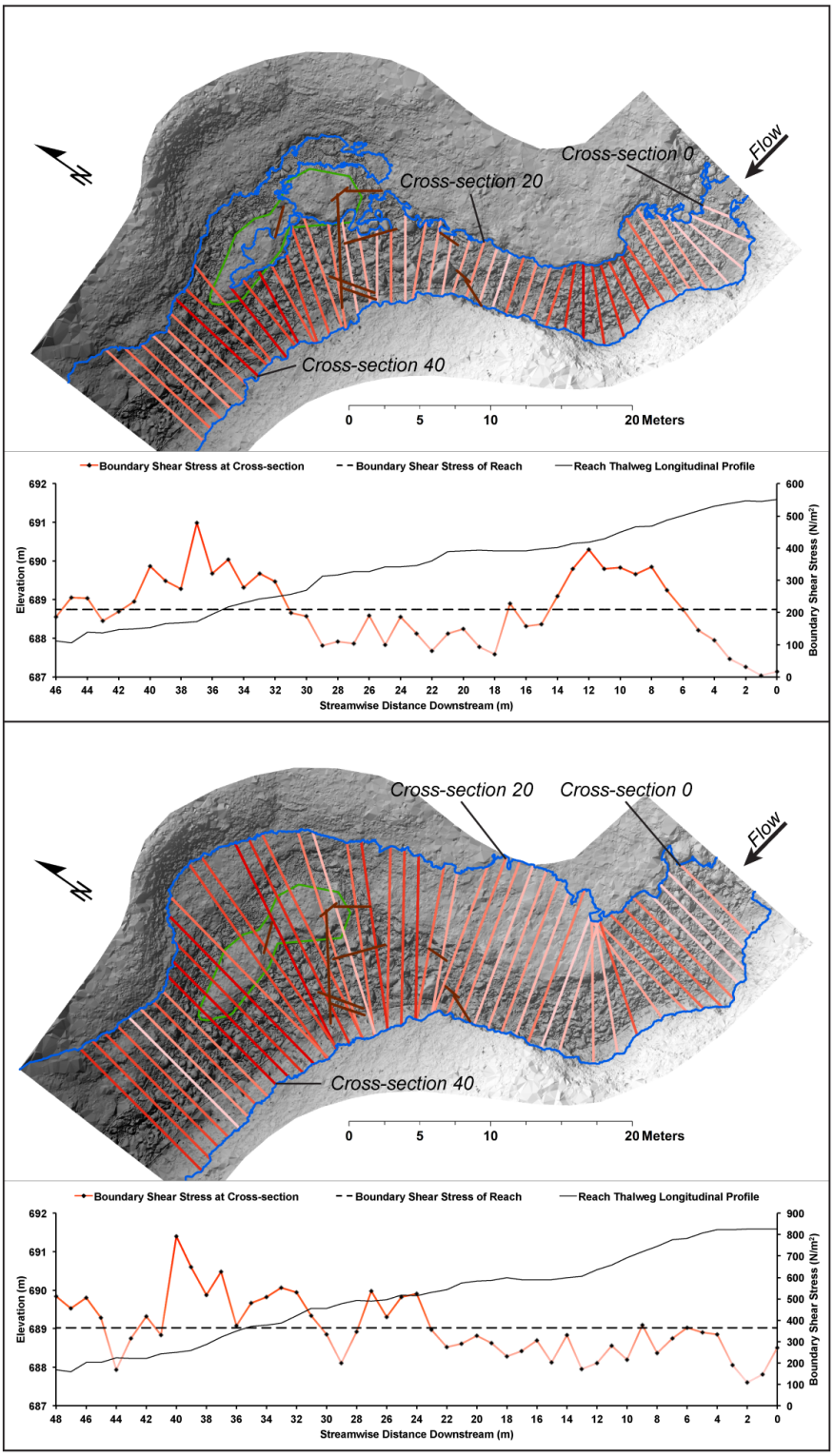

Figure 7. Boundary shear stress variation in reach A at low (top) and high (bottom) flow conditions. For figures 7 through 10: lateral flow extent is indicated by the blue line; mid-channel bar perimeter is given by the green line; instream wood distribution is given by the brown lines; shear stress or stream power magnitudes are given by the correlation between the gradient lines of the DEM overlay and the subjacent graph. Note that, in both reaches, the series of cross-sections for each flow condition do not begin in the same place due to differences in channel centerline and inundation.

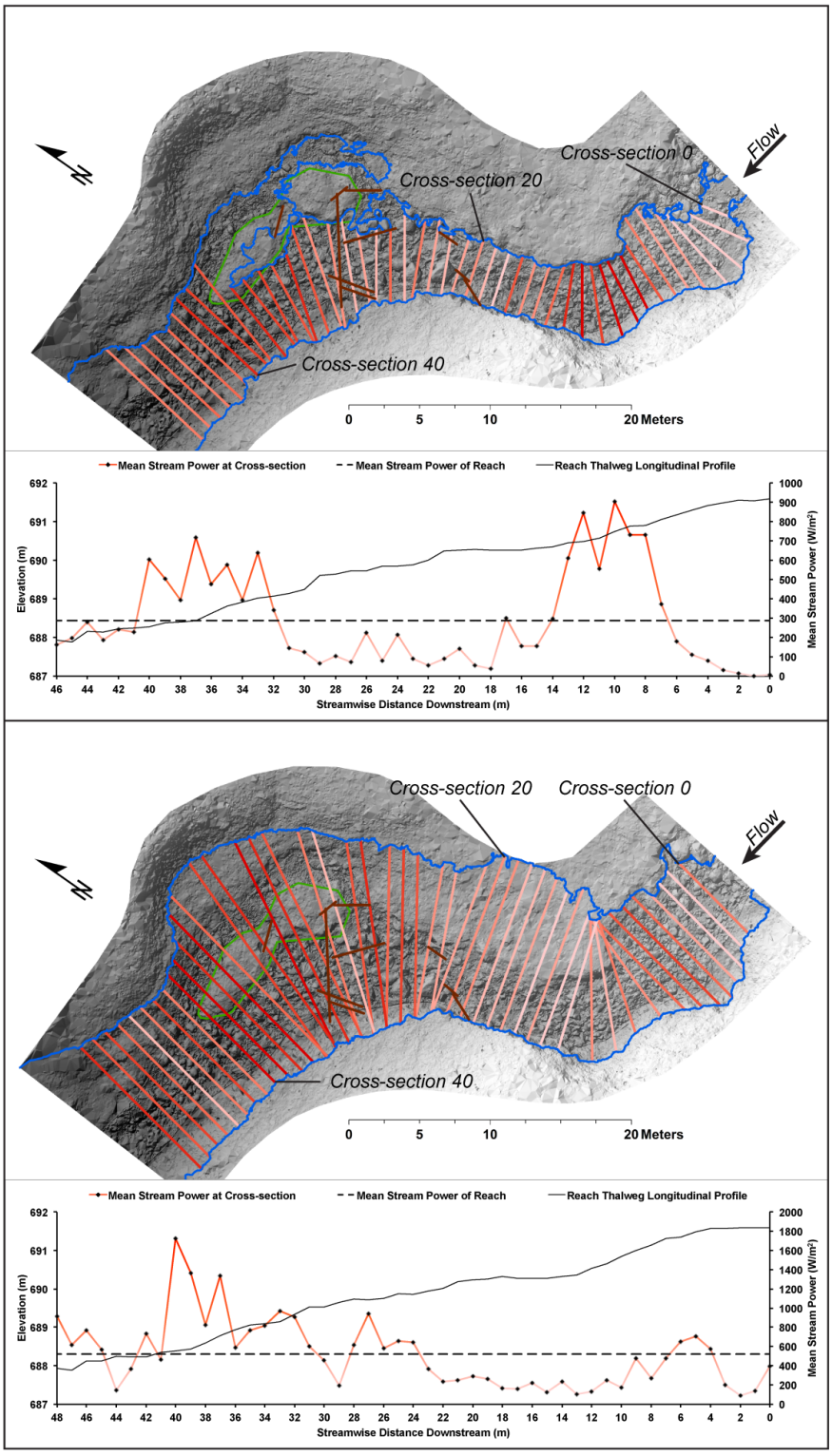

Figure 8. Mean Stream Power variation in reach A at low (top) and high (bottom) flow conditions.

straight stepped-bed morphology recorded in the downstream-most cross-sections. Mean values of τ and ω for the population of reach A cross-sections at low flow are 208.7 N/m^2 and 287.5 W/m^2, with standard deviations of 108.2 N/m^2 and 245.4 W/m^2, respectively. At high flow, mean values of τ and ω are 364.1 N/m^2 and 521.0 W/m^2, with standard deviations of 143.2 N/m^2 and 355.1 W/m^2, respectively.

Reach B profiles of τ and ω also mimic one another. Like reach A, reach B cross-sections begin in an upstream pool; however, the step-pool sequence continues through the meander bend (Figures 9, 10, cross-sections 0-32). The first "pool-step" sequence can be clearly resolved at both flow levels. Subsequent steps and pools are only clearly discernable at high flow with corresponding increases and decreases in τ and ω (Figures 9, 10, bottom, cross-sections 0-32). The thalweg profile clearly correlates steps with peaks in both hydraulic variables through this sequence. At low flow, τ and ω vary significantly through the subsequent step-pools, where the highest values of each occur, but do not show the quasi-regular profile seen at the high flow condition (Figures 9, 10, top, cross-sections 9-30). Again, lateral margin and mid-channel bar inundation spatially correlate with slight differences between the hydraulic profiles of the low and high flow conditions. At high flow, the greatest values of τ and ω occur in between the meander bend and bifurcation (cross-sections 30-50) and correspond with very steep bed slopes for those cross-sections ($\approx$ 16%). At low flow, the hydraulic profile of this area exhibits a step-pool pattern, similar to that seen in upstream reach A. Over the bar (Figures 9, 10, bottom, cross-sections 52-69), τ and ω values correspond with a longitudinal bar surface slope change from an upstream to a downstream dip. Around the bar

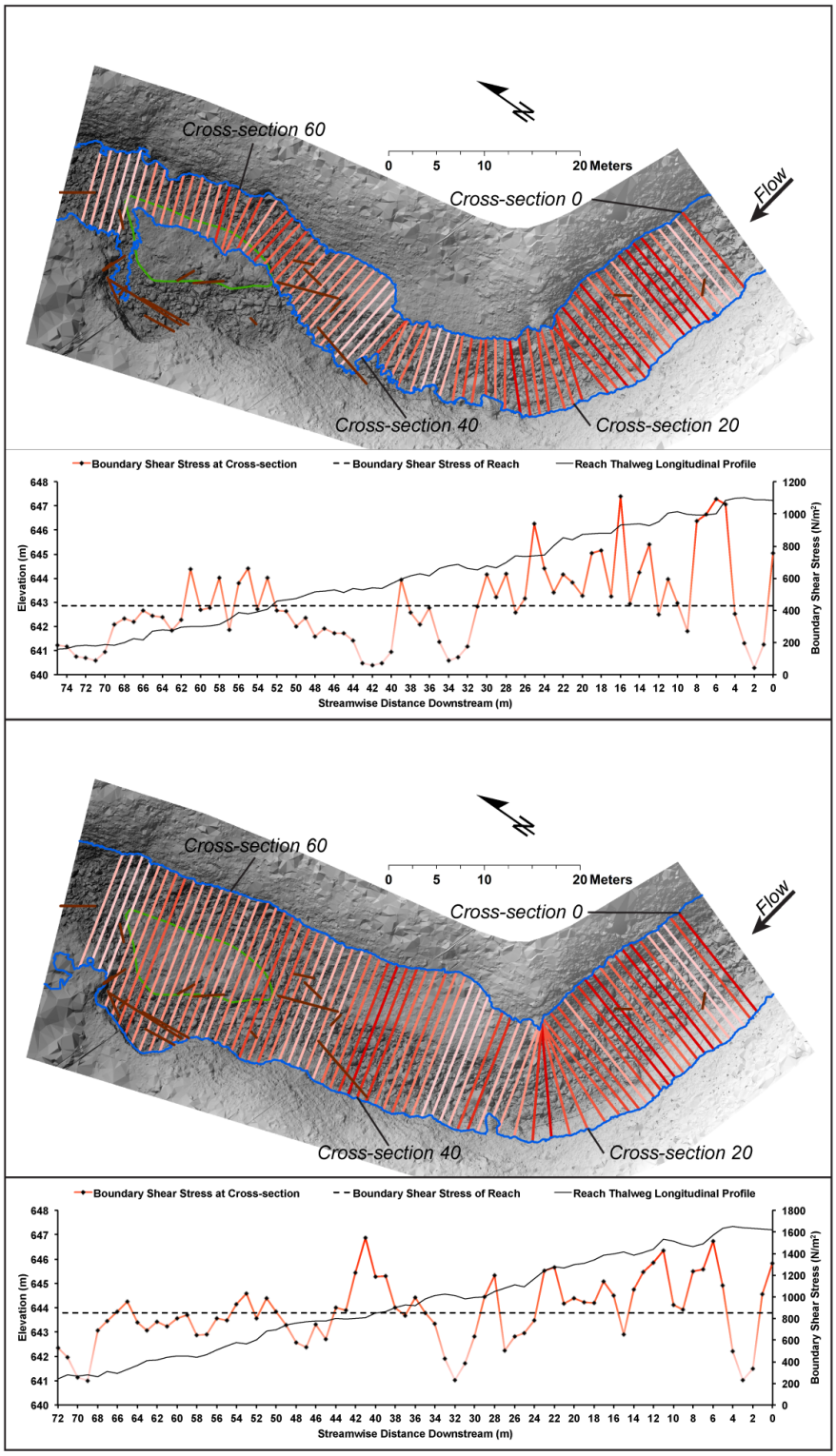

Figure 9. Boundary shear stress variation in reach B at low (top) and high (bottom) flow conditions

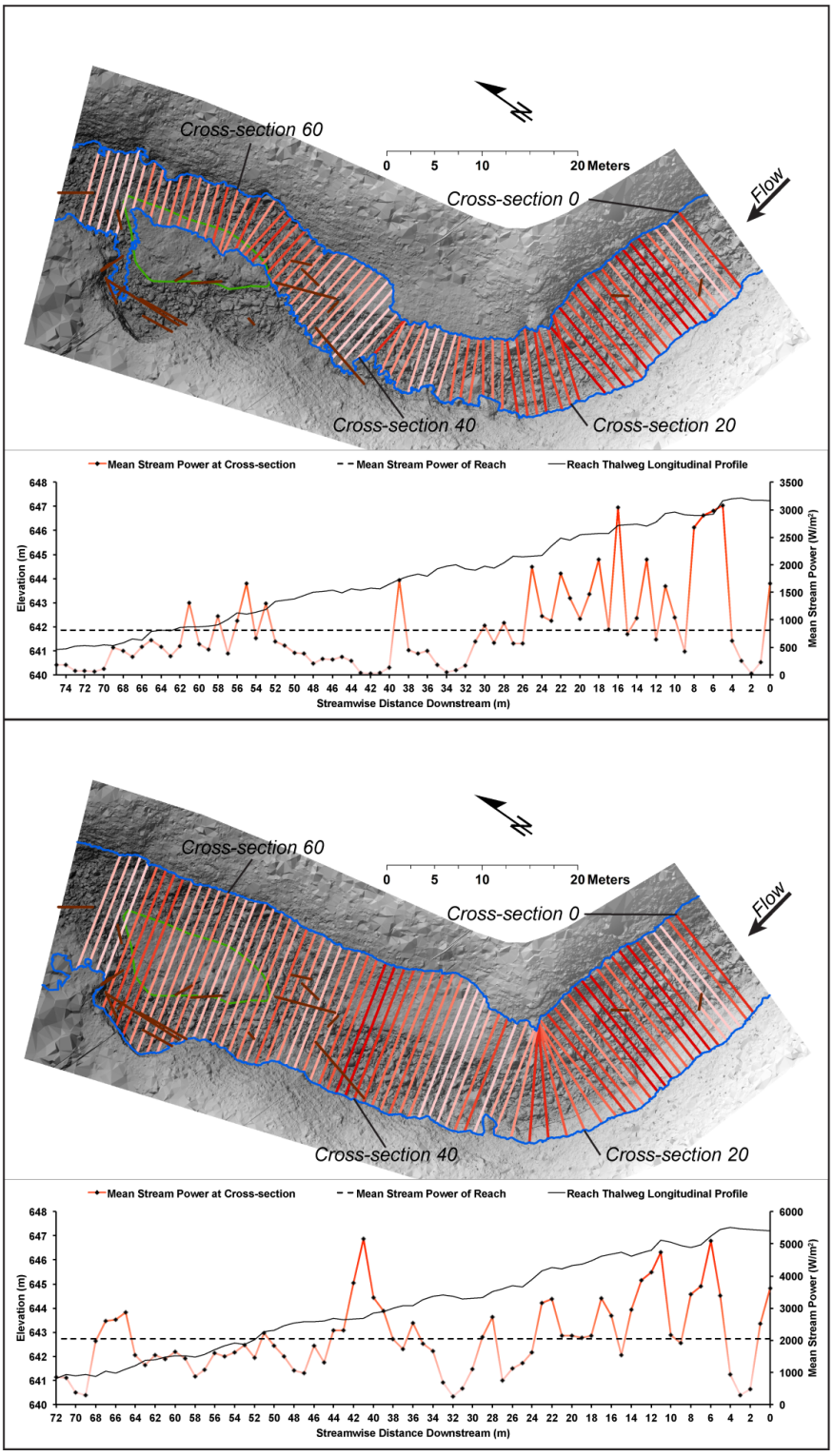

Figure 10. Mean Stream Power variation in reach A at low (top) and high (bottom) flow conditions.

(Figures 9, 10, top, cross-sections 51-71), τ and ω exhibit a similar, noisy profile pattern to that seen in the step-pool sequences upstream. Mean values of τ and ω for the population of reach B cross-sections at low flow are 429.1 N/m^2 and 811.1 W/m^2, with standard deviations of 258.4 N/m^2 and 773.5 W/m^2, respectively. At high flow, mean values of τ and ω are 852.5 N/m^2 and 2045.2 W/m^2, with standard deviations of 302.7 N/m^2 and 1125.6 W/m^2, respectively.

Step-wise regressions for high and low flow levels in both reaches show that S accounts for the highest fraction of mean stream power (ω) variability followed by σ_z, with p values << 0.001 for both variables. S also accounted for the highest fraction of variability in boundary shear stress (τ) in all scenarios except for the low flow condition in reach A, where R was slightly more accountable. S and R have p values << 0.001 in all shear stress step-wise regression models. Between reaches, bed morphometry denotes a downstream trend of increasing d, R, S and σ_z for each flow level, based on reach-averaged values. This is mathematically related to increasing magnitude, range, and variation of τ and ω, and corresponds with increasing downstream step height, channel width/depth, and maximum grain size observed in the field.

4.3. Reach Instream Wood

The spatial distribution of instream wood, given by piece length and spatial arrangement, is superimposed over the cross-sections for both flow levels in each reach. This helps to highlight morphometric trends in piece deposition. Reach A and

B contained 10 and 19 individual wood pieces, respectively, with abundance / loading values of 22.54 (pieces/100m), 2.28 (m^3/100m) and 19.03 (pieces/100m), 1.71 (m^3/100m), respectively. No pieces are deposited in the secondary bifurcation channel in reach A, while a large portion of the instream wood is deposited there in reach B. No pieces fall within the upstream step-pools in reach A. In reach B, one small unattached piece occurs in a pool while another rests on the upstream face of a step. In reach A, some pieces are resting on the upstream side of large boulders. Instream wood distribution in both reaches demonstrate that piece deposition is spatially related to the presence of an impendence in the form of channel morphology (bifurcation, mid-channel bar, secondary channels), bed material, or another wood piece.

5. Discussion

5.1. Variable Accountability in Hydraulic Prediction

Discharge, slope, and relative submergence have been found to be the best predictors of resistance, and therefore velocity, in steep mountain streams (Comiti et al., 2007; David et al., 2010; Afzalimehr et al., 2011; Yochum et al., 2012). Statistical analysis here demonstrates that S is the most predictive variable followed by σ_z for hydraulic calculations. This is expected since velocity was calculated using the relative submergence relationship (d/σ_z, Equation 2) put forth by Yochum et al. (2012), and that discharge was not a direct input into the ω calculation. Our confidence in the accuracy of the DEMs is reinforced by the high fraction of accountability of S and σ_z. Golden and Springer (2006) distinguished a strong statistical relationship between S, D_{50}, and ω across multiple channel morphologies (primarily cascades and step-pools), using a dataset of 157 high-gradient, temperate stream reaches. This higher-resolution study is in agreement with their findings, using σ_z as a measure of flow resistance.

5.2. Interpretation of Model Results with Field Observations

A distinctive hydraulic pattern exists for the upstream step-pools under high flow conditions. We believe this hydraulic signature is related to the transition from subcritical to supercritical flow over the steps, and back to subcritical flow in the

pools (Zimmerman et al., 2010) as both τ and ω peak over the steps and bottom through the pools. Flow depth over steps is typically less than that of pools. The modeled high flow condition, however, transports a large hydraulic radius of water at high velocity over the steps to generate extremely high τ and ω values (1514 N/m^2 and 5100 W/m^2, Figures 9, 10, bottom, respectively, cross-section 6). This spike in stream power over the steps demonstrates these step-pool sequences to be an effective means of kinetic modulation, as energy must be greatly expended to generate these high stream power values (Chin and Phillips, 2007). Reach segments that fall between individual step-pools or step-pool sequences are hydraulically distinguished by the lack of a diagnostic pattern. At high flow, this is likely a result of the lateral margin and mid-channel bar inundation significantly influencing S and σ_z values through topographic variability. At low flow, this effect is lessened, but transitional cascade morphologies occurring through the meander bends and/or bifurcation are still only hydraulically identified by their proximity to step-pools. Though step-pools can be hydraulically resolved in 1D, cascades may require a 2D or 3D model space to reveal distinguishable flow behavior.

The frequencies of storm events that produce flow regimes similar to those modeled are unknown. Turowski et al. (2009) found that two flow events occurring 23 years apart (with 40-50 year return periods) were capable of redistributing step-pools for a stream in a similar sized, albeit temperate, basin. Reckling et al. (2012) found that return periods for step-remobilizing flows to be as low as 20 years for 25 mountain streams reaches in the Vosges and Alps, France. Tropical basins are generally characterized as experiencing seasonal high intensity-short duration-high

frequency storm events; however, flow regime magnitudes are largely dependent on the nature of basin response. Riparian evidence of high-magnitude events may be difficult to distinguish given the elevated rates of bio-productivity in tropical ecosystems. The modeled high flow condition is likely capable of rearranging the channel bed morphology since its elevation is based on evidence of the highest flow level seen in the field. Similar magnitude flows may occur with return periods of less than 20 years; however, field evidence is largely destroyed through subsequent events and biotic recovery. Estimation of effective return periods in the absence of a discharge record is difficult in high-energy systems. Additional research is needed in tropical basins to link storm intensity, duration and frequency with flow regime and bed mobility.

The distribution of instream wood relative to physical impedance can indicate the nature of the depositing flow. Unattached pieces seen deposited on the upstream side of bed boulders indicates that their deposition occurred under a flow condition that did not fully inundate these grains. This level could represent the peak or the waning portion of a flow event. This also applies to wood pieces seen imbricated against the mid-channel bars; though, it is unlikely that flow significantly overtop the bars given their fine sediment accumulation in a channel otherwise devoid of considerable sediment accommodation.

5.3. Model Caveats

Reach A and B were selected for surveying and modeling because they displayed a complex arrangement of morphological elements that are in part a response to, but will subsequently influence, flow regime. For reaches of a single morphology type, extreme care is given to channel geometry measurements because geometric errors easily propagate through models and calculations of resistance and velocity (Lee and Ferguson, 2002; Comiti et al., 2007). Abrupt transitions between morphologies necessitate the same level of care especially since "bankfull" channel geometry can be difficult to distinguish in transitional channel segments. Using TLS to generate the input DEMs for our model provides the densest, most accurate surface from which to measure geometries. This importance is further accentuated because no direct flow measurements exist with which to calibrate hydraulic calculations.

Modeling a single time event flow in an ungauged stream necessitates some considerations when determining input parameters and analyzing results. For this study, flow levels were based off of field stage indicators. This calibrates the model to site-specific conditions, but it does not imply that the selected flow levels are responsible for the present configuration of the bed material or substrate. Resultant hydraulic indices represent flows that interact with the bed at an initial instant. Flow over time could theoretically rearrange the bed and present new hydraulic conditions. It is not feasible, then, to interpret the modeled hydraulic conditions as

the driving force behind the present morphological arrangement. These modeled results are reacting to the morphology represented by the input DEMs.

Reach averaged mean cross-sectional depth for the high flow condition in reach A and B is 0.66m and 1.25m, respectively. At these depths, flow levels significantly encroach upon the lateral margins inside the meander bends and extend over the mid-channel bars (Figures 7 through 10, bottom). Because DEM generation requires a bare-channel surface, the flow resistance imparted by riparian and bar vegetation is not fully captured by cross-sectional geometries. DEMs are longitudinally detrended; however, lateral margin slope is retained and affects σ_z. Consequently, roughness measurements that consider lateral margins incorporate a roughness component derived from the margin's slope. This component is directly related to the steepness, regularity, and extent of the inundated margin; however, it is not known how this component of roughness compares to the actual vegetation roughness of these same margins. Reach averaged mean cross-sectional depth for the low flow condition in reach A and B is 0.39m and 0.64m, respectively (Figures 7 through 10, top). Here, flow does not significantly extend up the lateral margins and bypasses the mid-channel bars, so that σ_z primarily reflects roughness derived from the channel substrate and bed material. We estimate that roughness is still under-predicted at high flow because of the highly irregular and non-uniform nature of riparian vegetation. Using σ_z as the measure of flow resistance quantifies form drag as water flows over an obstacle; however, riparian vegetation imparts a proportion of its resistance as water flows around the obstacle. Thought the resistive effects of vegetative irregularities are quantifiable (Kean and Smith, 2006), our consideration

of roughness only accounts for the resistance imparted by the topographic variation of the bare channel bed and margins.

When considering the modeled hydraulic conditions in relation to instream wood distribution, note that neither modeled flow level is explicitly responsible for the present distribution of wood pieces nor is it determined whether or not the flow condition would mobilize any particular piece. The high flow condition is likely capable of transporting any particular unattached piece, given their deposition on the mid-channel bars. Mobility of attached pieces (only ramps were field identified in these two reaches) at the high flow condition is less discernable given the unknown nature of their connection to the bank. The low flow condition cannot interact with any piece that is not placed within the low flow boundary; however, this flow still may not be capable of transporting eligible unattached pieces since no field evidence is seen to indicate transport capacity at this particular flow level. Also, the type of wood occurrence can change given variable flow level. Field classifications of instream wood were made in relation to riparian indicators of channel bank geometry. Flows that exceed this geometry may interact with attached instream wood pieces (bridges and ramps) as if they were unattached, notwithstanding rootwad attachment.

5.4. Stream-Scale Implications

Reach averaged roughness (σ_z), S, and width increase within the distance between Reach A and B. Additionally, observed maximum grain size, channel width

and incision increase with downstream distance for the entire channel length, while bedrock substrate lithology does not vary. The stream does confluence with first-order tributaries, which can elevate downstream erosive capability and contribute additional coarse sediment. Increased channel incision may also be related to the predominance of virgin forests in the lower reaches of the basin. Well-established riparian vegetation can confine channel margins thereby reducing storage capacity (Golden and Springer, 2006). Confined flows coupled with tributary additions impart more stress and expend greater amounts of energy against the channel margins, and are more capable of transporting larger grains, incising into bedrock substrates and flushing finer sediments.

Connectivity to available sources of fine sediment depends on the proximity of the source and the transport capacity of the flow regime. Storage of fine sediment is primarily accomplished via mid-channel bars, and minimal storage is seen in large pools. This sediment is likely derived from numerous riparian slope failures, the largest of which occurs in between reach A and B (Figure 11). The uppermost mapped reach morphology is alluvial. Here, the channel is set into coarse sand to fine gravel sediments and displays regular meanders and immature flood plain development. The sediment source for this reach is identified as a private property located immediately upstream (Figure 12). The property spans a few hundred meters of the upper stream length with a gentle gradient. It has been cleared of rainforest and has two ponds created by impounding the stream. Though a significant portion of the riparian slope sediment is stored in the ponds, a large fraction of the sediment is flushed downstream, creating the alluvial reach. The

Figure 11. Riparian slope failure located between reaches A and B. *Top* – Slump scarp. *Bottom* – Slump toe intersecting the channel margins. Field book for scale.

Figure 12. Uppermost portion of the study stream. *Top* – Cleared private property with numerous slumps located immediately upstream of alluvial reach. *Center* – Alluvial reach meander, photo taken after rainstorm. *Bottom* – Abrupt transition from alluvial to straight stepped-bed morphology, given by the presence of boulders.

transition to the subsequent, straight stepped-bed morphology is sharp and indicates that any sediment flushed past this boundary is subsequently transferred through the entire system, barring storage in a mid-channel bar or pool. No evidence is seen elsewhere in the basin to suggest an alluvial reach could be maintained without an immediate and abundant source.

The remaining morphology types can indicate downstream trends in flow regime and bed material availability. The magnitude of any storm event is distributed along the length of the stream. Compared to the upper portion of the stream, the lower stream course conveys higher-magnitude flows because of increased drainage area, tributary contribution, and channel incision. These large flows are the most capable means of step-pool sequence formation, maintenance, and re-distribution (Chin and Wohl, 2005) as shown by progressively well-developed, periodic step-pool sequences distributed downstream (Figure 5). Their regular arrangement utilizes and distributes the observed downstream increase in grain size variability into a contemporaneous, rhythmic adjustment between regime hydraulics and channel bed form (Chin, 2002). This tropical HWS presents another level of flow complexity as vertical flow vectors are distorted when step-pools are maintained through channel meanders. This is possible due to weakened lateral confinement from intense bedrock weathering, so that the channel uses three dimensions to modulate flow energy within a step-pool sequence. The presence of stepped-bed morphologies upstream indicate that flows are not consistently capable of arranging the available bed material into a continuous, efficient, defined form. This is also reflected in the short morphology-reach lengths of the upper

stream portion. Bifurcated reaches demonstrate the ultimate and immediate necessity of hydraulic modulation when vertical adjustments are insufficient. This morphology is bound by either stepped-bed or step-pool reaches and represents a chaotic response to excessive flow stress and power. Initial channel widening and/or meandering attenuates flow energy and competence so that the flow must deposit entrained material while synonymously partitioning around settling particles. The flow can then re-occupy a narrower channel while imparting boundary energies that can once again be regulated by vertical adjustments. We speculate that bifurcated reaches represent a transitional morphology assemblage between vertically controlled reaches (stepped-bed and step-pool), and that they form in response to flow regime exceeding a critical hydraulic threshold of lateral erosion.

Increases in instream wood piece size, abundance, and loading are consistent with the increasing channel width, transport capacity, and a downstream progression from young (10-20 year) second growth forests to pristine rainforest (Ozenick, 2010). In the lower course of the stream, large trees can contribute more and larger wood pieces to the channel, especially bridges and ramps. More massive pieces will be preferentially retained through increases hydraulic transport capacity. Also, unattached pieces flushed from upstream can congregate behind large boulders, larger wood pieces, or mid-channel bars. The lack of vine-entangled pieces downstream is likely related to the channel width and flow regime preventing riparian vines from growing within channel margins.

6. Conclusions

Modeled hydraulic conditions at the morphology-scale prove to be a powerful tool in understanding reach-scale fluvial interactions when coupled with rigorous field classifications. Channel bifurcation and unattached instream wood occurrences distinguish portions of the stream that represent transitional flow regimes set apart from rhythmic bed adjustments. TLS is able to capture the topographic complexity of these reaches at an unprecedented resolution, providing the best possible surfaces for fluvial simulations. One-dimensional hydraulic modeling resolves channel-spanning morphologies and serves as a hydraulic reference for links made between channel morphology, flow regime and (in)organic bed material distribution. Downstream trends in morphology and instream wood show that variation in flow magnitude, riparian environment, and sediment availability interact to produce compounding morphological expressions that necessitate further research into tropical HWS systems using multi-dimensional modeling. Not every HWS can be monitored; however, multi-faceted field investigations amplify the interpretative capabilities of models designed to characterize them. This study demonstrates the prominence of fluvial interconnectivity and complexity within a tropical HWS, and the results support continued innovation of developed geomorphological methods to better classify, survey, and interpret complex fluvial systems.

APPENDIX

Appendix 1*: Reach A Low Flow Data Table*

Cross-section	XSLength (m)	Extension (m)	StatSep (m)	NumStat	BFElev (m)	γ (N/m^3)	P (m)	A (m^2)	R (m)	d (m)	S	σ_z (m)	u (m/s)	V (m/s)	τ (N/m^2)	ω (W/m^2)
0	4.326	1	0.05	88	97.698	9810	2.414	0.184	0.076	0.101	0.022	0.047	0.147	0.312	16.334	5.102
1	6.739	1	0.05	136	97.672	9810	4.247	0.327	0.077	0.093	0.006	0.044	0.074	0.155	4.549	0.706
2	7.268	1	0.05	147	97.704	9810	5.832	0.842	0.144	0.169	0.023	0.069	0.193	0.477	31.884	15.194
3	8.626	1	0.05	174	97.687	9810	7.949	1.023	0.129	0.164	0.045	0.081	0.269	0.543	56.694	30.788
4	8.410	1	0.05	170	97.699	9810	8.013	1.426	0.178	0.230	0.065	0.125	0.385	0.707	114.293	80.828
5	8.913	1	0.05	180	97.702	9810	9.248	1.574	0.170	0.228	0.086	0.132	0.439	0.757	143.879	108.892
6	8.709	1	0.05	176	97.690	9810	8.312	2.042	0.246	0.305	0.087	0.182	0.510	0.854	209.237	178.645
7	6.891	1	0.05	139	97.700	9810	6.879	2.067	0.300	0.422	0.091	0.187	0.614	1.388	268.335	372.332
8	6.345	1	0.05	128	97.703	9810	6.002	2.280	0.380	0.524	0.092	0.168	0.687	2.138	341.957	731.014
9	6.973	1	0.05	141	97.690	9810	7.436	2.667	0.359	0.539	0.091	0.163	0.693	2.290	319.863	732.328
10	7.444	1	0.05	150	97.716	9810	8.196	3.476	0.424	0.644	0.082	0.174	0.719	2.654	340.623	904.027
11	7.729	1	0.05	156	97.682	9810	7.491	3.596	0.480	0.626	0.071	0.250	0.661	1.653	335.157	554.162
12	7.408	1	0.05	150	97.738	9810	8.001	3.767	0.471	0.698	0.086	0.249	0.765	2.143	394.867	846.212
13	6.678	1	0.05	135	97.706	9810	7.217	2.802	0.388	0.603	0.088	0.240	0.722	1.816	335.617	609.387
14	6.512	1	0.05	132	97.669	9810	6.190	2.436	0.393	0.541	0.065	0.268	0.586	1.185	249.652	295.763
15	6.073	1	0.05	123	97.665	9810	5.438	2.235	0.411	0.588	0.041	0.305	0.485	0.936	164.249	153.671
16	6.029	1	0.05	122	97.598	9810	5.035	2.061	0.409	0.558	0.039	0.257	0.462	1.000	156.430	156.476
17	6.280	1	0.05	127	97.786	9810	5.840	2.545	0.436	0.585	0.053	0.245	0.553	1.324	227.712	301.509
18	6.062	1	0.05	123	97.701	9810	5.117	1.485	0.290	0.367	0.025	0.204	0.299	0.536	70.599	37.829
19	6.238	1	0.05	126	97.716	9810	5.620	1.244	0.221	0.297	0.042	0.169	0.351	0.615	92.184	56.694
20	6.266	1	0.05	127	97.708	9810	5.003	1.416	0.283	0.333	0.054	0.149	0.419	0.936	149.350	139.778
21	6.011	1	0.05	122	97.693	9810	5.013	0.733	0.146	0.191	0.094	0.118	0.419	0.676	134.789	91.184
22	6.407	1	0.05	130	97.522	9810	2.937	0.281	0.096	0.155	0.087	0.085	0.364	0.660	81.601	53.872
23	7.352	1	0.05	149	97.687	9810	6.033	0.926	0.154	0.221	0.090	0.148	0.441	0.660	134.966	89.118
24	7.684	1	0.05	155	97.677	9810	7.291	1.573	0.216	0.322	0.088	0.147	0.527	1.153	186.175	214.737
25	8.255	1	0.05	167	97.697	9810	7.555	1.123	0.149	0.230	0.068	0.114	0.393	0.796	99.617	79.301
26	7.271	1	0.05	147	97.726	9810	7.212	1.722	0.239	0.325	0.081	0.142	0.510	1.170	190.708	223.116
27	7.211	1	0.05	146	97.748	9810	7.192	1.145	0.159	0.214	0.066	0.111	0.372	0.720	102.713	73.927
28	7.417	1	0.05	150	97.672	9810	6.338	0.745	0.118	0.165	0.095	0.070	0.393	0.927	110.050	102.060
29	8.882	1	0.05	179	97.687	9810	8.197	0.967	0.118	0.180	0.084	0.101	0.385	0.687	97.032	66.673
30	9.654	1	0.05	195	97.721	9810	7.922	1.391	0.176	0.243	0.109	0.189	0.510	0.654	188.010	123.048
31	10.297	1	0.05	207	97.701	9810	9.428	1.891	0.201	0.291	0.101	0.212	0.536	0.736	197.911	145.732
32	10.271	1	0.05	207	97.704	9810	9.698	2.529	0.261	0.308	0.116	0.158	0.591	1.157	295.555	341.894
33	13.913	1	0.05	280	97.709	9810	8.175	2.477	0.303	0.375	0.108	0.119	0.630	1.994	320.798	639.712
34	13.903	1	0.05	280	97.695	9810	8.508	2.327	0.273	0.375	0.104	0.164	0.618	1.414	278.197	393.492
35	13.102	1	0.05	264	97.735	9810	8.703	3.030	0.348	0.489	0.107	0.221	0.716	1.581	365.099	577.082
36	12.016	1	0.05	242	97.662	9810	8.178	2.521	0.308	0.435	0.106	0.197	0.672	1.483	320.278	474.837
37	11.860	1	0.05	239	97.695	9810	7.861	3.380	0.430	0.524	0.113	0.266	0.763	1.502	477.912	717.753
38	10.863	1	0.05	219	97.682	9810	11.848	4.245	0.358	0.482	0.078	0.204	0.607	1.436	273.560	392.767
39	9.901	1	0.05	200	97.702	9810	11.143	4.418	0.396	0.559	0.077	0.215	0.649	1.690	298.463	504.418
40	10.099	1	0.05	203	97.717	9810	10.720	5.070	0.473	0.626	0.074	0.240	0.674	1.759	343.130	603.471
41	9.370	1	0.05	189	97.696	9810	9.166	3.775	0.412	0.514	0.058	0.287	0.541	0.969	234.570	227.393
42	9.381	1	0.05	189	97.700	9810	8.767	4.025	0.459	0.544	0.045	0.225	0.490	1.185	202.809	240.344
43	9.533	1	0.05	192	97.701	9810	8.940	4.375	0.489	0.580	0.036	0.244	0.454	1.077	173.774	187.188
44	9.726	1	0.05	196	97.700	9810	9.045	4.131	0.457	0.537	0.055	0.252	0.537	1.142	245.282	280.094
45	10.351	1	0.05	209	97.697	9810	9.876	4.172	0.422	0.500	0.059	0.340	0.540	0.792	246.252	195.147
46	11.447	1	0.05	230	97.699	9810	10.935	4.800	0.439	0.508	0.043	0.271	0.466	0.873	187.270	163.549

***Appendix 2**: Reach A High Flow Data Table*

Cross-section	XSLength (m)	Extension (m)	StatSep (m)	NumStat	BFElev (m)	γ (N/m^3)	P (m)	A (m^2)	R (m)	d (m)	S	σ_z (m)	u (m/s)	V (m/s)	τ (N/m^2)	ω (W/m^2)
0	9.043	1	0.05	182	98.266	9810	8.959	3.143	0.351	0.452	0.079	0.186	0.593	1.443	272.451	393.027
1	9.659	1	0.05	195	98.307	9810	8.958	3.640	0.406	0.473	0.036	0.209	0.411	0.932	145.206	135.286
2	10.590	1	0.05	213	98.315	9810	10.658	4.415	0.414	0.513	0.027	0.231	0.368	0.815	108.968	88.853
3	10.753	1	0.05	217	98.299	9810	10.243	4.748	0.464	0.543	0.041	0.239	0.470	1.067	188.491	201.064
4	12.111	1	0.05	244	98.310	9810	11.980	6.289	0.525	0.623	0.065	0.225	0.628	1.737	332.779	578.007
5	11.848	1	0.05	238	98.298	9810	12.178	6.681	0.549	0.678	0.064	0.215	0.652	2.060	343.472	707.610
6	11.401	1	0.05	230	98.298	9810	11.650	6.802	0.584	0.724	0.064	0.270	0.671	1.798	363.801	654.079
7	10.929	1	0.05	220	98.297	9810	11.037	6.341	0.574	0.712	0.056	0.293	0.626	1.520	315.850	480.205
8	10.475	1	0.05	211	98.302	9810	10.445	6.276	0.601	0.743	0.042	0.374	0.551	1.094	245.418	268.562
9	10.507	1	0.05	212	98.296	9810	10.749	6.516	0.606	0.762	0.063	0.414	0.688	1.267	376.567	477.234
10	11.469	1	0.05	231	98.301	9810	11.798	7.265	0.616	0.769	0.035	0.501	0.517	0.793	213.835	169.599
11	12.061	1	0.05	243	98.300	9810	12.839	8.331	0.649	0.825	0.044	0.555	0.596	0.885	279.550	247.515
12	11.678	1	0.05	235	98.302	9810	12.021	6.808	0.566	0.702	0.036	0.514	0.495	0.677	197.853	133.892
13	11.962	1	0.05	241	98.301	9810	12.041	6.860	0.570	0.690	0.031	0.507	0.456	0.621	172.044	106.817
14	13.563	1	0.05	273	98.254	9810	13.203	6.149	0.466	0.549	0.072	0.476	0.624	0.720	330.605	238.104
15	12.795	1	0.05	257	98.293	9810	13.505	6.329	0.469	0.594	0.044	0.481	0.508	0.627	203.326	127.507
16	13.541	1	0.05	272	98.249	9810	13.070	6.622	0.507	0.589	0.061	0.478	0.595	0.733	304.918	223.381
17	13.954	1	0.05	281	98.272	9810	13.476	5.706	0.423	0.482	0.062	0.419	0.539	0.620	255.836	158.582
18	14.037	1	0.05	282	98.273	9810	14.031	5.488	0.391	0.457	0.060	0.331	0.520	0.719	231.485	166.345
19	13.931	1	0.05	280	98.353	9810	14.344	6.467	0.451	0.541	0.066	0.359	0.593	0.895	292.824	262.131
20	13.925	1	0.05	280	98.265	9810	12.644	5.412	0.428	0.483	0.078	0.325	0.607	0.901	325.946	293.743
21	13.072	1	0.05	263	98.323	9810	13.483	4.853	0.360	0.431	0.082	0.300	0.590	0.848	289.961	246.027
22	12.118	1	0.05	244	98.294	9810	13.938	4.299	0.308	0.426	0.091	0.305	0.617	0.862	275.510	237.395
23	13.174	1	0.05	265	98.296	9810	13.506	4.877	0.361	0.447	0.101	0.290	0.664	1.026	356.120	365.493
24	13.642	1	0.05	274	98.311	9810	13.761	6.216	0.452	0.534	0.118	0.342	0.787	1.228	524.162	643.462
25	14.442	1	0.05	290	98.305	9810	14.948	5.755	0.385	0.462	0.135	0.280	0.781	1.290	508.481	656.081
26	14.962	1	0.05	301	98.295	9810	16.393	7.146	0.436	0.550	0.097	0.286	0.724	1.392	415.393	578.410
27	15.432	1	0.05	310	98.300	9810	16.169	8.687	0.537	0.646	0.102	0.296	0.804	1.755	537.257	943.086
28	15.796	1	0.05	317	98.302	9810	17.078	8.010	0.469	0.580	0.075	0.211	0.653	1.795	344.364	618.159
29	17.089	1	0.05	343	98.300	9810	18.591	7.936	0.427	0.526	0.047	0.264	0.495	0.984	198.691	195.489
30	17.361	1	0.05	349	98.295	9810	19.413	7.875	0.406	0.515	0.083	0.242	0.649	1.382	332.069	458.882
31	18.139	1	0.05	364	98.295	9810	19.846	7.994	0.403	0.495	0.107	0.250	0.720	1.424	422.291	601.336
32	18.258	1	0.05	367	98.296	9810	20.749	9.394	0.453	0.578	0.119	0.276	0.821	1.722	528.373	909.725
33	18.261	1	0.05	367	98.309	9810	20.221	10.583	0.523	0.651	0.107	0.308	0.829	1.751	551.827	966.426
34	18.616	1	0.05	374	98.296	9810	20.072	11.335	0.565	0.683	0.092	0.333	0.784	1.609	508.973	818.817
35	18.941	1	0.05	380	98.295	9810	19.720	10.953	0.555	0.646	0.088	0.302	0.746	1.598	478.893	765.450
36	17.984	1	0.05	361	98.295	9810	18.730	10.947	0.584	0.686	0.065	0.287	0.662	1.585	373.097	591.206
37	16.626	1	0.05	334	98.272	9810	17.987	10.611	0.590	0.729	0.108	0.300	0.880	2.138	626.331	1338.792
38	14.806	1	0.05	298	98.298	9810	17.129	9.858	0.576	0.753	0.092	0.389	0.823	1.591	518.430	824.949
39	13.542	1	0.05	272	98.312	9810	14.930	10.441	0.699	0.904	0.095	0.394	0.916	2.100	648.601	1361.869
40	12.844	1	0.05	258	98.293	9810	14.140	9.283	0.656	0.856	0.123	0.399	1.016	2.179	791.750	1725.172
41	12.539	1	0.05	252	98.304	9810	13.903	9.990	0.719	0.951	0.047	0.453	0.663	1.391	331.512	461.233
42	12.242	1	0.05	246	98.307	9810	13.826	10.538	0.762	1.033	0.056	0.439	0.751	1.767	416.185	735.343
43	12.850	1	0.05	258	98.303	9810	13.408	9.403	0.701	0.863	0.046	0.459	0.621	1.167	313.779	366.211
44	13.099	1	0.05	263	98.299	9810	12.754	9.582	0.751	0.863	0.023	0.435	0.439	0.871	168.001	146.357
45	13.099	1	0.05	263	98.305	9810	13.068	10.030	0.768	0.900	0.055	0.453	0.694	1.379	411.090	566.781
46	13.312	1	0.05	268	98.298	9810	12.852	10.048	0.782	0.889	0.066	0.442	0.758	1.524	505.532	770.659
47	13.869	1	0.05	279	98.303	9810	14.403	10.272	0.713	0.863	0.065	0.474	0.741	1.351	454.054	613.418
48	14.175	1	0.05	285	98.300	9810	14.418	11.165	0.774	0.919	0.067	0.400	0.778	1.789	509.968	912.133

***Appendix 3**: Reach B Low Flow Data Table*

Cross-section	XSLength (m)	Extension (m)	StatSep (m)	NumStat	BFElev (m)	γ (N/m^3)	P (m)	A (m^2)	R (m)	d (m)	S	σ_z (m)	u (m/s)	V (m/s)	τ (N/m^2)	ω (W/m^2)
0	12.393	1	0.05	249	95.196	9810	13.987	11.791	0.843	1.139	0.092	0.528	1.012	2.186	758.134	1657.050
1	12.764	1	0.05	257	95.191	9810	13.510	12.635	0.935	1.170	0.021	0.457	0.486	1.242	188.498	234.093
2	12.729	1	0.05	256	95.193	9810	13.781	11.610	0.842	1.085	0.005	0.382	0.231	0.656	41.381	27.144
3	12.968	1	0.05	261	95.209	9810	14.216	11.146	0.784	1.018	0.025	0.399	0.502	1.283	194.252	249.164
4	13.246	1	0.05	266	95.195	9810	14.928	10.828	0.725	0.967	0.053	0.421	0.709	1.629	376.846	613.939
5	13.375	1	0.05	269	95.182	9810	14.415	11.813	0.820	1.041	0.132	0.415	1.161	2.907	1060.403	3082.936
6	13.109	1	0.05	264	95.199	9810	15.553	11.750	0.756	1.054	0.147	0.478	1.235	2.723	1093.064	2976.469
7	12.932	1	0.05	260	95.199	9810	14.654	13.781	0.940	1.259	0.108	0.503	1.156	2.896	999.225	2893.507
8	12.983	1	0.05	261	95.205	9810	15.484	13.823	0.893	1.262	0.109	0.524	1.162	2.799	955.380	2673.845
9	12.913	1	0.05	260	95.200	9810	14.753	12.735	0.863	1.163	0.032	0.450	0.605	1.564	271.694	425.003
10	12.940	1	0.05	260	95.199	9810	14.260	12.470	0.874	1.144	0.052	0.372	0.762	2.342	443.333	1038.417
11	13.204	1	0.05	266	95.196	9810	15.375	11.298	0.735	1.009	0.082	0.335	0.903	2.720	593.683	1614.727
12	13.589	1	0.05	273	95.195	9810	14.805	12.237	0.827	1.059	0.046	0.429	0.693	1.711	374.956	641.416
13	13.700	1	0.05	276	95.201	9810	15.393	12.596	0.818	1.077	0.101	0.431	1.034	2.580	812.182	2095.422
14	13.824	1	0.05	278	95.201	9810	14.245	10.696	0.751	0.903	0.086	0.485	0.873	1.625	634.603	1031.377
15	13.189	1	0.05	265	95.204	9810	15.469	10.953	0.708	0.982	0.063	0.454	0.780	1.691	439.090	742.342
16	13.000	1	0.05	261	95.208	9810	13.368	10.523	0.787	0.957	0.144	0.405	1.161	2.742	1109.816	3043.007
17	12.220	1	0.05	246	95.199	9810	14.599	8.580	0.588	0.837	0.085	0.411	0.833	1.697	487.345	826.978
18	11.184	1	0.05	225	95.198	9810	12.261	8.870	0.723	0.969	0.109	0.363	1.016	2.714	771.022	2092.226
19	11.570	1	0.05	233	95.204	9810	12.242	7.432	0.607	0.778	0.127	0.395	0.985	1.941	756.278	1467.851
20	10.486	1	0.05	211	95.176	9810	11.329	6.721	0.593	0.795	0.084	0.311	0.810	2.073	488.781	1013.291
21	10.942	1	0.05	220	95.226	9810	11.768	7.124	0.605	0.796	0.096	0.282	0.867	2.448	571.875	1399.779
22	10.700	1	0.05	215	95.175	9810	12.384	5.801	0.468	0.667	0.136	0.212	0.942	2.967	622.675	1847.314
23	11.306	1	0.05	228	95.198	9810	14.477	5.052	0.349	0.552	0.149	0.259	0.899	1.918	510.573	979.035
24	10.496	1	0.05	211	95.199	9810	10.197	5.735	0.562	0.740	0.120	0.426	0.932	1.619	659.732	1068.096
25	9.819	1	0.05	198	95.156	9810	9.711	5.005	0.515	0.705	0.186	0.384	1.134	2.085	940.198	1960.262
26	9.472	1	0.05	191	95.217	9810	9.599	4.550	0.474	0.599	0.102	0.383	0.772	1.206	472.420	569.732
27	8.477	1	0.05	171	95.099	9810	8.244	3.932	0.477	0.629	0.083	0.308	0.714	1.460	386.534	564.485
28	8.027	1	0.05	162	95.217	9810	8.018	3.870	0.483	0.640	0.132	0.388	0.911	1.503	626.322	941.237
29	8.939	1	0.05	180	95.203	9810	9.524	3.807	0.400	0.552	0.123	0.374	0.816	1.206	482.653	581.886
30	8.458	1	0.05	171	95.200	9810	8.383	3.860	0.460	0.594	0.138	0.373	0.897	1.428	624.445	891.894
31	9.221	1	0.05	186	95.202	9810	9.081	4.998	0.550	0.694	0.078	0.352	0.731	1.441	423.705	610.349
32	9.033	1	0.05	182	95.180	9810	8.113	4.194	0.517	0.626	0.034	0.293	0.459	0.982	173.986	170.844
33	7.853	1	0.05	159	95.206	9810	7.224	2.535	0.351	0.433	0.031	0.203	0.363	0.775	106.857	82.823
34	9.073	1	0.05	183	95.200	9810	9.035	1.871	0.207	0.269	0.042	0.161	0.334	0.558	85.567	47.758
35	9.241	1	0.05	186	95.191	9810	9.400	2.215	0.236	0.341	0.087	0.203	0.541	0.909	201.992	183.691
36	9.533	1	0.05	192	95.198	9810	9.186	2.649	0.288	0.408	0.147	0.294	0.766	1.064	414.690	441.232
37	8.200	1	0.05	165	95.199	9810	7.706	2.036	0.264	0.326	0.121	0.165	0.622	1.228	313.578	385.217
38	8.405	1	0.05	170	95.197	9810	8.147	2.712	0.333	0.424	0.118	0.256	0.701	1.161	386.087	448.294
39	6.875	1	0.05	139	95.255	9810	6.701	3.016	0.450	0.616	0.134	0.190	0.899	2.918	590.078	1721.566
40	8.535	1	0.05	172	95.121	9810	8.266	2.459	0.298	0.403	0.049	0.193	0.441	0.921	143.200	131.939
41	10.145	1	0.05	204	95.176	9810	10.336	3.076	0.298	0.385	0.024	0.243	0.300	0.475	69.738	33.145
42	11.673	1	0.05	235	95.222	9810	12.017	3.534	0.294	0.364	0.020	0.261	0.268	0.374	58.041	21.717
43	11.224	1	0.05	226	95.211	9810	10.737	3.445	0.321	0.374	0.023	0.233	0.288	0.464	71.242	33.062
44	12.161	1	0.05	245	95.200	9810	12.064	3.405	0.282	0.336	0.077	0.138	0.502	1.220	211.938	258.574
45	11.591	1	0.05	233	95.200	9810	11.862	3.484	0.294	0.365	0.089	0.165	0.566	1.254	257.787	323.217
46	11.194	1	0.05	225	95.207	9810	11.256	3.794	0.337	0.412	0.078	0.209	0.560	1.106	256.654	283.782
47	11.029	1	0.05	222	95.224	9810	10.629	3.792	0.357	0.419	0.082	0.242	0.580	1.003	286.699	287.665
48	10.457	1	0.05	211	95.194	9810	10.347	3.016	0.292	0.375	0.083	0.246	0.553	0.844	237.923	200.768
49	9.431	1	0.05	190	95.215	9810	9.022	3.229	0.358	0.433	0.101	0.257	0.655	1.106	354.151	391.843
50	7.847	1	0.05	158	95.232	9810	8.911	2.493	0.280	0.476	0.109	0.253	0.713	1.343	299.372	402.052
51	8.544	1	0.05	172	95.204	9810	8.469	3.218	0.380	0.491	0.106	0.260	0.714	1.349	394.329	532.022
52	8.336	1	0.05	168	95.192	9810	8.537	3.174	0.372	0.500	0.110	0.243	0.734	1.510	400.575	604.810
53	8.217	1	0.05	166	95.203	9810	7.880	3.581	0.454	0.573	0.135	0.232	0.872	2.157	603.026	1300.901
54	7.894	1	0.05	159	95.202	9810	9.649	3.726	0.386	0.632	0.108	0.319	0.817	1.620	408.138	661.255
55	8.337	1	0.05	168	95.097	9810	7.862	4.121	0.524	0.687	0.128	0.255	0.931	2.506	660.524	1655.081
56	8.468	1	0.05	171	95.175	9810	8.478	4.129	0.487	0.651	0.119	0.330	0.872	1.718	568.735	977.292
57	8.636	1	0.05	174	95.200	9810	8.591	5.099	0.593	0.773	0.048	0.341	0.603	1.365	279.375	381.480
58	8.171	1	0.05	165	95.203	9810	8.317	4.471	0.538	0.721	0.114	0.365	0.899	1.777	602.280	1070.115
59	8.849	1	0.05	178	95.190	9810	9.019	3.399	0.377	0.496	0.113	0.336	0.741	1.093	417.147	455.974
60	8.986	1	0.05	181	95.197	9810	9.390	4.408	0.469	0.644	0.087	0.348	0.743	1.373	402.657	552.987
61	8.285	1	0.05	167	95.189	9810	7.618	4.390	0.576	0.708	0.116	0.319	0.898	1.994	655.990	1307.863
62	8.022	1	0.05	162	95.200	9810	7.453	3.479	0.467	0.575	0.074	0.244	0.647	1.526	339.970	518.783
63	7.384	1	0.05	149	95.198	9810	6.833	2.849	0.417	0.528	0.067	0.253	0.588	1.225	273.020	334.317
64	7.780	1	0.05	157	95.197	9810	7.449	2.785	0.374	0.484	0.098	0.232	0.682	1.425	358.456	510.839
65	7.619	1	0.05	154	95.201	9810	6.843	2.826	0.413	0.505	0.090	0.197	0.669	1.718	365.752	628.362
66	7.629	1	0.05	154	95.194	9810	7.117	2.600	0.365	0.464	0.112	0.261	0.713	1.270	399.827	507.720
67	6.949	1	0.05	140	95.208	9810	5.970	1.874	0.314	0.379	0.106	0.237	0.627	1.004	326.320	327.646
68	7.319	1	0.05	148	95.186	9810	6.332	2.272	0.359	0.429	0.099	0.222	0.647	1.251	349.772	437.503
69	7.362	1	0.05	149	95.208	9810	6.755	2.547	0.377	0.476	0.084	0.186	0.628	1.605	312.243	501.229
70	6.919	1	0.05	140	95.063	9810	5.908	1.387	0.235	0.292	0.061	0.155	0.418	0.790	139.877	110.490
71	11.272	1	0.05	227	95.196	9810	11.815	2.763	0.234	0.299	0.038	0.146	0.332	0.683	86.523	59.058
72	10.936	1	0.05	220	95.200	9810	10.343	2.385	0.231	0.268	0.047	0.132	0.350	0.714	105.512	75.344
73	10.590	1	0.05	213	95.195	9810	9.685	1.690	0.175	0.229	0.065	0.127	0.383	0.691	111.628	77.135
74	10.265	1	0.05	207	95.218	9810	9.483	2.208	0.233	0.285	0.077	0.132	0.463	1.003	175.162	175.674
75	9.592	1	0.05	193	95.218	9810	10.495	2.053	0.196	0.257	0.096	0.129	0.491	0.978	183.527	179.486

***Appendix 4**: Reach B High Flow Data Table*

Cross-section	XSLength (m)	Extension (m)	StatSep (m)	NumStat	BFElev (m)	γ (N/m^3)	P (m)	A (m^2)	R (m)	d (m)	S	σ_z (m)	u (m/s)	V (m/s)	τ (N/m^2)	ω (W/m^2)
0	15.207	1	0.05	306	96.198	9810	17.854	23.552	1.319	1.784	0.101	0.864	1.332	2.751	1312.236	3609.801
1	15.606	1	0.05	314	96.199	9810	16.949	25.112	1.482	1.847	0.070	0.851	1.129	2.451	1023.184	2507.777
2	15.741	1	0.05	316	96.210	9810	16.526	24.768	1.499	1.808	0.023	0.817	0.634	1.402	332.916	466.844
3	15.495	1	0.05	311	96.204	9810	16.774	23.679	1.412	1.754	0.017	0.726	0.535	1.293	230.541	298.111
4	16.051	1	0.05	323	96.201	9810	18.381	23.860	1.298	1.698	0.039	0.723	0.805	1.890	494.752	935.329
5	15.933	1	0.05	320	96.199	9810	18.318	23.765	1.297	1.710	0.087	0.672	1.206	3.069	1103.711	3387.541
6	16.197	1	0.05	325	96.197	9810	19.155	24.397	1.274	1.718	0.121	0.729	1.429	3.369	1513.920	5099.694
7	15.887	1	0.05	319	96.205	9810	19.960	25.517	1.278	1.836	0.100	0.840	1.342	2.931	1253.341	3673.710
8	15.971	1	0.05	321	96.188	9810	19.621	26.194	1.335	1.878	0.094	0.893	1.318	2.772	1234.395	3422.252
9	16.234	1	0.05	326	96.199	9810	18.438	25.595	1.388	1.796	0.065	0.884	1.069	2.172	883.373	1918.664
10	16.286	1	0.05	327	96.206	9810	18.677	25.264	1.353	1.767	0.070	0.836	1.100	2.325	926.863	2154.730
11	15.856	1	0.05	319	96.207	9810	18.544	24.049	1.297	1.736	0.112	0.721	1.382	3.326	1426.700	4745.876
12	16.253	1	0.05	327	96.210	9810	18.943	25.610	1.352	1.797	0.099	0.762	1.324	3.120	1318.127	4112.746
13	16.093	1	0.05	323	96.197	9810	17.824	25.751	1.445	1.833	0.087	0.729	1.249	3.138	1229.788	3859.235
14	16.133	1	0.05	324	96.197	9810	18.247	24.472	1.341	1.729	0.081	0.735	1.173	2.759	1067.288	2944.857
15	16.115	1	0.05	324	96.199	9810	20.580	23.108	1.123	1.633	0.059	0.677	0.975	2.350	653.185	1534.951
16	15.846	1	0.05	318	96.188	9810	17.631	22.662	1.285	1.636	0.080	0.682	1.135	2.723	1012.652	2757.319
17	15.304	1	0.05	308	96.202	9810	17.203	21.163	1.230	1.585	0.095	0.669	1.215	2.882	1146.023	3302.446
18	14.914	1	0.05	300	96.201	9810	17.294	19.853	1.148	1.533	0.084	0.762	1.123	2.260	944.044	2133.127
19	14.362	1	0.05	289	96.204	9810	17.087	18.271	1.069	1.479	0.091	0.780	1.147	2.176	950.151	2067.396
20	14.110	1	0.05	284	96.201	9810	15.819	17.234	1.089	1.424	0.093	0.751	1.138	2.157	990.585	2137.089
21	14.174	1	0.05	285	96.200	9810	17.211	16.710	0.971	1.375	0.098	0.693	1.152	2.285	936.459	2139.659
22	14.050	1	0.05	283	96.203	9810	16.126	16.037	0.994	1.331	0.130	0.671	1.304	2.588	1270.579	3288.366
23	14.402	1	0.05	290	96.204	9810	17.561	15.901	0.905	1.282	0.140	0.670	1.327	2.539	1243.052	3155.497
24	13.657	1	0.05	275	96.201	9810	16.421	15.622	0.951	1.347	0.084	0.692	1.054	2.052	784.583	1610.011
25	13.933	1	0.05	280	96.201	9810	20.109	16.164	0.804	1.358	0.084	0.747	1.060	1.929	665.443	1283.664
26	12.902	1	0.05	260	96.204	9810	14.548	13.116	0.902	1.203	0.072	0.629	0.922	1.763	636.276	1122.060
27	14.307	1	0.05	288	96.200	9810	16.839	13.028	0.774	1.059	0.066	0.589	0.828	1.487	500.486	744.394
28	14.668	1	0.05	295	96.189	9810	15.625	13.970	0.894	1.104	0.136	0.591	1.216	2.273	1196.902	2720.419
29	15.270	1	0.05	307	96.197	9810	16.975	14.717	0.867	1.107	0.118	0.599	1.130	2.089	1000.834	2091.189
30	15.286	1	0.05	307	96.203	9810	16.655	15.361	0.922	1.155	0.070	0.593	0.891	1.734	634.251	1100.086
31	16.203	1	0.05	326	96.207	9810	18.091	16.173	0.894	1.139	0.044	0.620	0.699	1.285	383.925	493.408
32	16.377	1	0.05	329	96.209	9810	17.572	15.089	0.859	1.048	0.028	0.507	0.533	1.101	232.671	256.237
33	17.300	1	0.05	347	96.199	9810	18.472	14.151	0.766	0.925	0.057	0.412	0.718	1.613	427.185	689.205
34	17.830	1	0.05	358	96.199	9810	18.646	14.365	0.770	0.906	0.099	0.383	0.940	2.223	750.526	1668.374
35	17.841	1	0.05	358	96.202	9810	20.117	15.057	0.748	0.953	0.116	0.443	1.040	2.235	849.003	1897.720
36	17.879	1	0.05	359	96.220	9810	20.198	15.435	0.764	0.974	0.132	0.427	1.124	2.565	991.355	2543.313
37	17.711	1	0.05	356	96.192	9810	19.482	14.282	0.733	0.910	0.115	0.439	1.011	2.097	823.974	1727.488
38	17.136	1	0.05	344	96.199	9810	18.585	14.577	0.784	0.965	0.117	0.451	1.053	2.255	900.457	2030.751
39	17.002	1	0.05	342	96.198	9810	19.789	13.868	0.701	0.925	0.174	0.475	1.255	2.443	1192.959	2914.872
40	16.631	1	0.05	334	96.196	9810	18.115	14.215	0.785	0.970	0.154	0.421	1.211	2.793	1186.726	3314.787
41	16.529	1	0.05	332	96.204	9810	18.011	16.975	0.942	1.167	0.167	0.482	1.382	3.343	1543.993	5161.302
42	16.615	1	0.05	334	96.205	9810	18.343	16.780	0.915	1.145	0.137	0.460	1.238	3.085	1224.961	3778.496
43	16.657	1	0.05	335	96.203	9810	17.364	17.087	0.984	1.166	0.091	0.454	1.020	2.618	877.408	2296.953
44	16.646	1	0.05	334	96.205	9810	18.188	16.438	0.904	1.122	0.101	0.464	1.056	2.555	898.907	2297.143
45	16.536	1	0.05	332	96.204	9810	18.064	16.441	0.910	1.134	0.068	0.464	0.873	2.133	611.622	1304.763
46	15.740	1	0.05	316	96.205	9810	16.527	16.148	0.977	1.174	0.078	0.453	0.948	2.459	747.628	1838.370
47	15.766	1	0.05	317	96.200	9810	17.536	14.501	0.827	1.055	0.066	0.473	0.826	1.840	534.712	983.765
48	15.838	1	0.05	318	96.196	9810	16.562	14.107	0.852	1.022	0.069	0.470	0.835	1.816	580.660	1054.709
49	16.059	1	0.05	323	96.203	9810	17.973	14.163	0.788	1.008	0.096	0.484	0.972	2.024	738.508	1494.775
50	16.542	1	0.05	332	96.196	9810	18.872	14.674	0.778	1.009	0.113	0.503	1.059	2.122	865.344	1836.598
51	17.233	1	0.05	346	96.255	9810	19.897	16.080	0.808	1.048	0.124	0.528	1.131	2.244	986.186	2213.033
52	17.514	1	0.05	352	96.178	9810	21.098	15.554	0.737	1.003	0.110	0.574	1.043	1.822	798.866	1455.141
53	17.953	1	0.05	361	96.209	9810	21.338	16.773	0.786	1.052	0.133	0.686	1.173	1.800	1029.089	1852.091
54	17.685	1	0.05	355	96.212	9810	20.802	16.472	0.792	1.049	0.120	0.672	1.111	1.734	931.284	1614.891
55	17.632	1	0.05	354	96.185	9810	20.620	17.272	0.838	1.107	0.095	0.594	1.018	1.898	783.489	1487.346
56	17.710	1	0.05	356	96.185	9810	20.174	17.380	0.862	1.104	0.095	0.565	1.014	1.979	802.975	1589.443
57	17.483	1	0.05	351	96.198	9810	19.860	15.635	0.787	1.012	0.084	0.554	0.915	1.670	651.145	1087.225
58	17.589	1	0.05	353	96.200	9810	20.323	15.163	0.746	0.972	0.088	0.650	0.916	1.369	644.238	882.205
59	18.496	1	0.05	371	96.254	9810	22.680	17.234	0.760	1.041	0.112	0.645	1.068	1.723	831.912	1433.297
60	18.962	1	0.05	381	96.295	9810	23.658	18.306	0.774	1.067	0.106	0.545	1.051	2.060	801.362	1650.797
61	20.327	1	0.05	408	96.224	9810	22.758	17.422	0.766	0.952	0.097	0.464	0.950	1.950	724.939	1413.349
62	20.616	1	0.05	414	96.241	9810	22.851	16.893	0.739	0.908	0.106	0.438	0.971	2.015	767.720	1547.014
63	20.819	1	0.05	418	96.211	9810	23.321	16.555	0.710	0.881	0.099	0.462	0.926	1.767	691.690	1222.123
64	20.371	1	0.05	409	96.196	9810	23.769	16.943	0.713	0.923	0.109	0.454	0.993	2.020	761.068	1537.638
65	19.581	1	0.05	393	96.219	9810	24.483	16.604	0.678	0.946	0.144	0.365	1.155	2.991	956.574	2860.885
66	19.095	1	0.05	383	96.202	9810	21.347	16.134	0.756	0.946	0.117	0.323	1.041	3.051	866.227	2642.846
67	18.488	1	0.05	371	96.196	9810	20.559	18.426	0.896	1.117	0.088	0.329	0.984	3.343	776.526	2595.644
68	17.943	1	0.05	360	96.210	9810	22.719	17.390	0.765	1.094	0.092	0.381	0.993	2.855	690.590	1971.653
69	14.872	1	0.05	299	96.199	9810	18.333	12.746	0.695	1.016	0.033	0.454	0.575	1.285	226.162	290.727
70	14.846	1	0.05	298	96.204	9810	15.665	13.608	0.869	1.059	0.030	0.411	0.558	1.440	255.745	368.193
71	13.768	1	0.05	277	96.201	9810	15.406	11.881	0.771	1.007	0.058	0.408	0.760	1.876	442.028	829.299
72	14.818	1	0.05	298	96.203	9810	15.671	12.123	0.774	0.943	0.070	0.477	0.804	1.591	530.559	844.221

Appendix 5*: Extended Stream Morphology and Instream Wood Table*

Reach ID	Morphology	Reach Length (m)	Bridge				Ramp				Unattached				Unattached-Emplaced				Vine-Entangled				Total			
			#	Vol. (m^3)	Abun. (#/100m)	Load. (m^3/100m)	#	Vol. (m^3)	Abun. (#/100m)	Load. (m^3/100m)	#	Vol. (m^3)	Abun. (#/100m)	Load. (m^3/100m)	#	Vol. (m^3)	Abun. (#/100m)	Load. (m^3/100m)	#	Vol. (m^3)	Abun. (#/100m)	Load. (m^3/100m)	#	Vol. (m^3)	Abun. (#/100m)	Load. (m^3/100m)
1	aluvial	186.93	8	1.77	4.28	0.95	15	0.37	8.02	0.20	9	0.17	4.81	0.09	3	0.16	1.60	0.0086	2	0.15	1.07	0.08	37	2.63	19.79	1.41
2	straight stepped-bed	68.78	0	---	---	---	0	---	---	---	0	---	---	---	0	---	---	---	0	---	---	---	0	---	---	---
3	bifurcated	24.10	1	0.02	4.15	0.08	0	---	---	---	1	0.02	4.15	0.10	0	---	---	---	1	0.01	4.15	0.05	3	0.06	12.45	0.23
4	straight stepped-bed	27.63	0	---	---	---	0	---	---	---	0	---	---	---	0	---	---	---	0	---	---	---	0	---	---	---
5	bifurcated	33.13	2	0.12	6.04	0.36	4	0.49	12.07	1.47	1	0.65	3.02	1.97	0	---	---	---	0	---	---	---	7	1.26	21.13	3.80
6	straight stepped-bed	27.35	0	---	---	---	0	---	---	---	3	0.05	10.97	0.19	0	---	---	---	0	---	---	---	3	0.05	10.97	0.19
7	bifurcated	18.25	0	---	---	---	0	---	---	---	1	0.05	5.48	0.30	0	---	---	---	0	---	---	---	1	0.05	5.48	0.30
8	step-pool	30.54	0	---	---	---	0	---	---	---	0	---	---	---	0	---	---	---	0	---	---	---	0	---	---	---
9	bifurcated	50.90	0	---	---	---	0	---	---	---	2	0.03	3.93	0.06	0	---	---	---	0	---	---	---	2	0.03	3.93	0.06
10	meandering stepped-bed	73.47	1	0.03	1.36	0.05	7	0.12	9.53	0.17	7	0.07	9.53	0.10	0	---	---	---	0	---	---	---	15	0.23	20.42	0.31
11	step-pool	84.39	1	0.09	1.18	0.11	6	0.54	7.11	0.63	1	0.01	1.18	0.01	0	---	---	---	1	0.03	1.18	0.04	9	0.68	10.66	0.80
12	bifurcated	41.78	0	---	---	---	0	---	---	---	0	---	---	---	0	---	---	---	1	0.01	2.39	0.03	1	0.01	2.39	0.03
13	straight stepped-bed	20.90	1	0.07	4.78	0.31	1	0.06	4.78	0.29	3	0.06	14.35	0.31	0	---	---	---	0	---	---	---	5	0.19	23.92	0.91
14	bifurcated	59.24	0	---	---	---	3	0.51	5.06	0.86	4	0.39	6.75	0.65	1	0.02	1.69	0.0285	1	0.37	1.69	0.62	9	1.29	15.19	2.18
15	step-pool	27.18	0	---	---	---	2	0.48	7.36	1.75	1	0.54	3.68	1.99	0	---	---	---	0	---	---	---	3	1.02	11.04	3.74
16	bifurcated	35.49	0	---	---	---	2	0.13	5.64	0.36	8	0.81	22.54	2.28	0	---	---	---	0	---	---	---	10	0.94	28.18	2.64
17	meandering stepped-bed	200.98	0	---	---	---	8	0.53	3.98	0.26	22	0.91	10.95	0.45	1	0.04	0.50	0.0025	6	0.41	2.99	0.21	37	1.89	18.41	0.94
18	step-pool	116.20	1	0.31	0.86	0.27	5	1.16	4.30	0.99	2	0.14	1.72	0.12	0	---	---	---	0	---	---	---	8	1.61	6.88	1.38
19	bifurcated	63.07	0	---	---	---	6	0.88	9.51	1.40	12	1.08	19.03	1.71	0	---	---	---	1	0.03	1.59	0.04	19	1.99	30.12	3.15
20	bifurcated	51.15	1	2.59	1.95	5.05	0	---	---	---	16	5.37	31.28	10.49	0	---	---	---	1	0.25	1.95	0.49	18	8.20	35.19	16.03
21	step-pool	154.24	1	0.45	0.65	0.29	5	1.58	3.24	1.02	15	1.71	9.72	1.11	0	---	---	---	1	0.09	0.65	0.06	22	3.83	14.26	2.48
22	bifurcated	76.23	0	---	---	---	5	5.39	6.56	7.07	27	3.80	35.42	4.99	0	---	---	---	0	---	---	---	32	9.20	41.98	12.06
23	step/pool	55.13	0	---	---	---	8	3.19	14.51	5.78	4	0.77	7.26	1.39	0	---	---	---	0	---	---	---	12	3.95	21.77	7.17
24	bifurcated	37.52	0	---	---	---	7	0.88	18.66	2.34	12	1.34	31.99	3.58	0	---	---	---	0	---	---	---	19	2.22	50.65	5.92
25	step-pool	52.60	0	---	---	---	3	6.96	5.70	13.24	8	3.41	15.21	6.49	0	---	---	---	0	---	---	---	11	10.38	20.91	19.72
26	bifurcated	107.81	1	3.94	0.93	3.66	5	22.85	4.64	21.19	28	5.45	25.97	5.05	0	---	---	---	0	---	---	---	34	32.24	31.54	29.91
27	step-pool	175.98	0	---	---	---	4	14.83	2.27	8.43	26	4.53	14.77	2.57	1	0.09	0.57	0.0032	0	---	---	---	31	19.45	17.62	11.05
28	bifurcated	61.81	0	---	---	---	8	3.56	12.94	5.76	20	2.59	32.35	4.18	0	---	---	---	0	---	---	---	28	6.14	45.30	9.94
29	step-pool	73.93	0	---	---	---	0	---	---	---	9	0.45	12.17	0.61	0	---	---	---	0	---	---	---	9	0.45	12.17	0.61
	Total	2036.71	18	9.397	0.88	0.46	104	64.493	5.11	3.17	242	34.414	11.88	1.69	6	0.321	0.29	0.0001	15	1.361	0.74	0.07	385	109.986	18.90	5.40

REFERENCES

Abbe, T.B., Montgomery, D.R., 1996. Large woody debris jams, channel hydraulics and habitat formation in large rivers. Regulated Rivers: Research and Management 12, 201-221.

Abbe, T.B., Montgomery, D.R., 2003. Patterns and processes of wood debris accumulation in the Queets river basin, Washington. Geomorphology 21, 81-107.

Afzalimehr, H., Gallichand, J., Sui, J., Bagheri, E., 2011. Field investigation on friction factor in mountainous cobble-bed and boulder-bed rivers. International Journal of Sediment Research 26, 210-221.

Aggett, G.R., Wilson, J.P., 2009. Creating and coupling a high resolution DTM with a 1-D hydraulic model in a GIS for scenario-based assessment of avulsion hazard in a gravel bed river. Geomorphology 113, 21-34.

Brooks, P.A., Brierley, G.J., 2002. Mediated equilibrium: the influence of riparian vegetation and wood on the long-term evolution and behavior of a near-pristine river. Earth Surface Processes and Landforms 27, 343-367.

Cadol, D., Wohl, E., Goode, J.R., Jaeger, K.L., 2009. Wood distribution in neotropical forested headwater streams of La Selva, Costa Rica. Earth Surface Processes and Landforms 34, 1198-1215.

Cadol, D., Wohl, E., 2010. Wood retention and transport in tropical, headwater streams, La Selva Biological Station, Costa Rica. Geomorphology 123, 61-73.

Cadol, D., Wohl, E., 2011. Coarse sediment movement in the vicinity of a logjam in a neotropical gravel-bed stream. Geomorphology 128, 191-198.

Caine, N., Mool, P.K., 1981. Channel Geometry and flow estimates for two small mountain streams in the Middle Hills, Nepal. Mountain Research and Development 1 (3/4), 231-243.

Cánovas, J.A.B., Eguibar, M., Bodoque, J.M., Díez-Herrero, A., Stoffel, M., Gutiérrez-Pérez, I., 2011. Estimating flash flood discharge in an ungauged mountain catchment with 2D hydraulic models and dendrogeomorphic paleostage indicators. Hydrological Processes 25, 970-979.

Chaplot, V., Darboux, F., Bourennane, H., Laguédois, S., Silvera, N., Phachomphon, K., 2006. Accuracy of interpolation techniques for the derivation of digital elevation models in relation to landform types and data density. Geomorphology 77, 126-141.

Chin, A., 2002. The periodic nature of step-pool mountain streams. American Journal of Science 302, 144-167.

Chin, A., Wohl, E., 2005. Toward a theory for step pools in stream channels. Progress in Physical Geography 29, 275-296.

Chin, A., Phillips, J.D., 2007. The self-organization of step-pools in mountain streams. Geomorphology 83, 346-358.

Comiti, F., Mao, L., Wilcox, A., Wohl, E.E., Lenzi, M.A., 2007. Field-derived relationships for flow velocity and resistance in high-gradient streams. Journal of Hydrology 340, 48-62.

Comiti, F., Mao, L., 2012. Recent advances on the dynamics of steep channels. In: Church, M., Biron, P., Roy, A.G. (Eds.), Gravel Bed Rivers 7: Processes, Tools, Environments. Wiley-Blackwell, Chichester, pp. 353–377.

Curran, J.C., 2012. Examining individual step stability within step-pool sequences. In: Church, M., Biron, P., Roy, A.G. (Eds.), Gravel Bed Rivers 7: Processes, Tools, Environments. Wiley-Blackwell, Chichester, pp. 378–385.

David, G.C.L., Wohl, E., Yochum, S.E., Bledsoe, B.P., 2010. Controls on spatial variations in flow resistance along a step mountain stream. Water Resources Research 46, W03513, doi: 10.1029/2009WR008134.

Dollar, E.S.J., 2002. Magnitude and frequency controlling fluvial sedimentary systems: issues, contributions and challenges. International symposium on the structure, function and management implications of fluvial sedimentary systems. IAHS-AISH, Australia, pp. 355-362.

Dollar, E.S.J., James, C.S., Rogers, K.H., Thoms, M.C., 2007. A framework for interdisciplinary understanding of river as ecosystems. Geomorphology 89, 147-162.

Erdogan, S., 2009. A comparison of interpolation methods for producing digital elevation models at the field scale. Earth Surface Processes and Landforms 34, 366-376.

Faustini, J.M., Jones, J.A., 2003. Influence of large woody debris on channel morphology and dynamics in steep, boulder-rich mountain streams, western Cascades, Oregon. Geomorphology 51, 187-205.

Ferguson, R.I., 2003. The missing dimension: effects of lateral variation on 1-D calculations of fluvial bedload transport. Geomorphology 56, 1-14.

Fetherston, K.L., Naiman, R.J., Bilby, R.E., 1995. Large woody debris, physical process, and riparian forest development in montane river networks of the Pacific Northwest. Geomorphology 13, 133-144.

Fonstad, M.A., 2003. Spatial variation in the power of mountain streams in the Sangre de Cristo Mountains, New Mexico. Geomorphology 55, 75-96.

Golden, L.A., Springer, G.S., 2006. Channel geometry, median grain size, and stream power in small mountain streams. Geomorphology 78, 64-76.

Grant, G.E., Swanson, F.J., Wolman, W.G., 1990. Pattern and origin of stepped-bed morphology in high-gradient streams, Western Cascades, Oregon. Geological Society of American Bulletin 102, 340-352.

Gurnell, A.M., Piégay, H., Swanson, F.J., Gregory, S.V., 2002. Large wood and fluvial processes. Freshwater Biology 47, 601-619.

Harrison, L.R., Keller, E.A., 2007. Modeling forced pool-riffle hydraulics in a boulder-bed stream, southern California. Geomorphology 83, 232-248.

Hattanji, T., Wasklewicz, T., Hayakawa, Y., Wester, T., Hegi, Y., 2012. Hydrogeomorphic effects of basin lithology on development of channel steps in first-order basins of the Ashio Mountains, Japan. Physical Geography 33 (6), 536-560.

Hengl, T., Evans, I.S., 2009. Mathematical and digital models of the land surface. In: Hengl, T., Reuter, H.I. (Eds.), Geomorphometry: Concepts, Software, Applications. Elsevier, Amsterdam, pp. 31–63.

Heritage, G., Hetherington, D., 2007. Towards a protocol for laser scanning in fluvial geomorphology. Earth Surface Processes and Landforms 32, 66-74.

Heritage, G.L., Milan, D.J., 2009. Terrestrial laser scanning of grain roughness in a gravel-bed river. Geomorphology 113, 4-11.

Heritage, G.L., Milan, D.J., Large, A.R.G., Fuller, I., 2009. Influence of survey strategy and interpolation model upon DEM quality. Geomorphology 112, 334-344.

Hodge, R., Brasington, J., Richards, K., 2009a. In situ characterization of grain-scale fluvial morphology using terrestrial laser scanning. Earth Surface Processes and Landforms 34, 954-968.

Hodge, R., Brasington, J., Richards, K., 2009b. Analyzing laser-scanned digital terrain models of gravel-bed surfaces: linking morphology to sediment transport processes and hydraulics. Sedimentology 56, 2024-2043.

Horritt, M.S., Bates, P.D., Mattinson, M.J., 2006. Effects of mesh resolution and topographic representation in 2D finite volume models of shallow water fluvial flow. Journal of Hydrology 329, 306-314.

Hyatt, T.L., Naiman, R.J., 2001. The residence time of large woody debris in the Queets River, Washington, USA. Ecological Applications 11 (1), 191-202.

Isenburg, M., Liu, Y., Shewchuk, J., Snoeyink, J., Thirion, T., 2006. Generating raster DEM from mass points via TIN streaming, GIScience'06 Conference Proceedings. Springer Berlin Heidelberg, Münster, Germany, pp. 186-198.

Jackson, C.R., Sturm, C.A., 2002. Woody debris and channel morphology in first- and second-order forested channels in Washington's coast ranges. Water Resources Research 38 (9), 1177-1191.

Jones, T.A., Daniels, L.D., Powell, S.R., 2011. Abundance and function of large woody debris in small, headwater streams in the Rocky Mountain foothills of Alberta, Canada. River Research and Applications 27, 297-311.

Kean, J.W., Smith, J.D., 2006. Form drag in rivers due to small-scale natural topographic features: 2. Irregular sequences. Journal of Geophysical Research 111, F04010, doi: 10.1029/2006JF000490.

Lane, S.N., Westaway, R.M., Hicks, D.M., 2003. Estimation of erosion and deposition volumes in a large gravel-bed, braided river using synoptic remote sensing. Earth Surface Processes and Landforms 28, 249-271.

Lee, A.J., Ferguson, R.I., 2002. Velocity and flow resistance in step-pool streams. Geomorphology 46, 59-71.

Massong, T.M., Montgomery, D.R., 2000. Influence of sediment supply, lithology, and woody debris on the distribution of bedrock and alluvial channels. Geological Society of America Bulletin 112 (5), 591-599.

Maue, T., Springer, M., 2008. Effect of methodology and sampling time on the taxa richness of aquatic macroinvertabrates and subsequent changes in the water quality index from three tropical rivers, Costa Rica. Revista de Biología Tropical 56, 257-271.

McCoy, S. W., Kean, J. W., Coe, J. A. , Staley, D. M. , Wasklewicz, T. A. , Tucker, G.E., 2010. Evolution of a natural debris flow: in situ measurements of flow dynamics, video imagery, and terrestrial laser scanning. Geology 38 (8), 735-738.

McKean, J., Nagel, D., Tonia, D., Baily, P., Wright, C.W., Bohn, C., Nayegandhi, A., 2009. Remote sensing of channels and riparian zones with a narrow-beam aquatic-terrestrial LiDAR. Remote Sensing 1, 1065-1096.

Milan, D.J., Heritage, G.L., Hetherington, D., 2007. Application of a 3-D laser scanner in the assessment of eroson and deposition volumes and channel change in a proglacial river. Earth Surface Processes and Landforms 32, 1657-1674.

Milan, D.J., Heritage, G.L., Large, A.R.G., Fuller, I.C., 2011. Filtering spatial error from DEMs: implications for morphological change estimation. Geomorphology 125, 160-171.

Milan, D.J., Heritage, G.L., 2012. LiDAR and ADCP use in gravel-bed rivers: Advances since GBR6. In: Church, M., Biron, P., Roy, A.G. (Eds.), Gravel Bed Rivers 7: Processes, Tools, Environments. Wiley-Blackwell, Chichester, pp. 286-302.

Montgomery, D.R., Buffington, J.M., 1997. Channel-reach morphology in mountain drainage basins. Geological Society of America Bulletin 109, 596-611.

Nakamura, F., Swanson, F.J., Wondzell, S.M., 2000. Disturbance regimes of stream and riparian systems – a disturbance-cascade perspective. Hydrological Processes 14, 2849-2860.

Nelson, P.A., Seminara, G., 2011. Modeling the evolution of bedrock channel shape with erosion from saltating bed load. Geophysical Research Letters 38, L17406, DOI: 10.1029/2011GL048628.

Ozenick, K. M., 2010. Structure and species composition of primary and secondary tropical forest in Costa Rica: a case study using ecosystem service payments for conservation of biodiversity. M.S. Thesis, Texas Christian University, 76 pp.

Piégay, H., Gurnell, A.M., 1997. Large woody debris and river geomorphological pattern: examples from S.E. France and S. England. Geomorphology 19, 99-116.

Pike, A.S., Scatena, F.N., 2010. Riparian indicators of flow frequency in a tropical montane stream network. Journal of Hydrology 382, 72-87.

Pike, A.S., Santena, F.N., Wohl, E.E., 2010. Lithological and fluvial controls on the geomorphology of tropical montane stream channels in Puerto Rico. Earth Surface Processes and Landforms 35 (12), 1402-1417.

Recking, A., Leduc, P., Liébault, F., Church, M., 2012. A field investigation of the influence of sediment supply on step-pool morphology and stability. Geomorphology 139-140, 53-66.

Reuter, H.I., Hengl, T. Gessler, P., Soille, P. 2009. Preparation of DEMs for geomorphometric analyses. In: Hengl, T., Reuter, H.I. (Eds.), Geomorphometry: Concepts, Software, Applications. Developments in Soil Science 33, Elsevier, Amsterdam, pp. 87-120.

Rychkov, I., Brasington, J., Vericat, D., 2012. Computational and methodological aspects of terrestrial surface analysis based on point clouds. Computers and Geosciences 42, 64-70.

Schürch, P., Densmore, A.L., Rosser, N, J., Lim, M., McArdell, B.W., 2011. Detection of surface change in complex topography using terrestrial laser scanning: application to the Illgraben debris-flow channel. Earth Surface Processes and Landforms 36, 1847-1859.

Schwendel, A.C., Fuller, I.C., Death, R.G., 2012. Assessing DEM interpolation methods for effective representation of upland stream morphology for rapid appraisal of bed stability. River Research and Applications 28, 567-584.

Smith, M., Vericat, D., Gibbins, C., 2012. Through-water terrestrial laser scanning of gravel beds at the patch scale. Earth Surface Processes and Landforms 37, 411-421.

Staley, D., Wasklewicz, T., Coe, J., Kean, J., McCoy, S., Tucker, G., 2011. Observations of debris flows at Chalk Cliffs, Colorado, USA: Part 2, changes in surface morphometry from terrestrial laser scanning in the summer of 2009. In Genevois, R., Hamilton, D.L., and Prestininzi, A (Eds.) Proceedings of the 5th International Conference on Debris Flow Hazards Mitigation, Mechanics, Prediction and Assessment, Padua, Italy, Rome, Italy: Italian Journal of Engineering Geology and Environment and Casa Editrice Universita La Sapienza, 759-768.

Turowski, J.M., Yager, E.M., Badoux, A., Rickenmann, D., Molnar, P., 2009. The impact of exceptional events on erosion, bedload transport and channel stability in a step-pool channel. Earth Surface Processes and Landforms 34, 1661-1673.

Wasklewicz, T.A., Hattanji, T., 2009. High-resolution analysis of debris flow-induced channel changes in a headwater stream, Ashio Mountains, Japan. The Professional Geographer 61 (2), 231-249.

Wheaton, J.M., Brasington, J, Darby, S.E., Sear, D.A., 2010. Accounting for uncertainty in DEMs from repeat topographic surveys: improved sediment budgets. Earth Surface Processes and Landforms 35, 136-156.

Wilcox, A.C., Wohl, E.E., 2006. Flow resistance in step-pool stream channels:1. Large woody debris and controls on total resistance. Water Resources Research 42, W05418, DOI: 10.1029/2005WR004277.

Wohl, E.E., 1995. Estimating flood magnitude in ungauged mountain channels, Nepal. Mountain Research and Development 15 (1), 69-76.

Wohl, E., 2005. Downstream hydraulic geometry along a tropical mountain river. In: Harmon, R.S. (Ed.), The Río Chagres, Panama. Springer, the Netherlands, pp. 169-188.

Wohl, E., Goode, J., 2008. Wood dynamics in headwater streams of the Colorado Rocky Mountains. Water Resources Research 44, W09429, DOI: 10.1029/2007WR006522.

Wohl, E., Merritt, D.M., 2008. Reach-scale channel geometry of mountain streams. Geomorphology 93, 168-185.

Wohl, E., Jaeger, K., 2009. A conceptual model for the longitudinal distribution of wood in mountain streams. Earth Surface Processes and Landforms 34, 329-344.

Wohl, E., Ogden, F.L., Goode, J., 2009. Episodic wood loading in a mountainous neotropical watershed. Geomorphology 111, 149-159.

Wohl, E., Polvi, Lina, E., Cadol, D., 2011. Wood distribution along streams draining old-growth floodplain forests in Congaree National Park, South Carolina, USA. Geomorphology 126, 108-120.

Wohl, E., Bolton, S., Cadol, D., Comiti, F., Goode, J.R., Mao, L., 2012. A two end-member model of wood dynamics in headwater neotropical rivers. Journal of Hydrology 462-463, 67-76.

Wooldridge, C.L., Hickin, E.J., 2002. Step-pool and cascade morphology, Mosquito Creek, British Columbia: a test of four analytical techniques. Canadian Journal of Earth Science 39, 493-503.

Yager, E.M., Kirchner, J.W., Dietritch, W.E., 2007. Calculating bed load transport in steep boulder bed channels. Water Resources Research 43, W07418, DOI: 10.1029/2006WR005432.

Yager, E.M., Dietrich, W.E., Kirchner, J.W., McArdell, B.W., 2012. Patch dynamics and stability in steep, rough streams. Journal of Geophysical Research 117, F02010, DOI: 10.1029/2011JF002253.

Yilmaz, I., 2009. A research on the accuracy of landform volumes determined using different interpolation methods. Scientific Research and Essay 4 (11), 1248-1259.

Yochum, S.E., Bledsoe, B.P., David, G.C.L., Wohl, E., 2012. Velocity prediction in high-gradient channels. Journal of Hydrology 424-425, 84-98.

Zimmerman, A., Church, M. Hassan, M.A., 2010. Step-pool stability: testing the jammed state hypothesis. Journal of Geophysical Research 115, F02008, doi: 10.1029/2009JF001365.

VITA

Peyton Lisenby was born on June 3rd, 1989 in Beaumont, Texas. He is the son of Curtis Lisenby and Lorette Sanborn. He graduated from Orangefield High School in Orangefield, Texas in 2007. He received his Bachelor of Science degree summa cum laude with a major in Geology and a minor in Geography from Sam Houston State University in Huntsville, Texas in 2010.

Peyton joined Texas Christian University for graduate study in August 2011 where he received his Masters of Science degree in Geology in 2013. During his time at TCU, Peyton assisted and taught Physical and Structural Geology labs, was inducted into Sigma Gamma Epsilon, received a Geological Society of America research grant and the Fort Worth Geological Society scholarship, and presented his thesis project results at the Geological Society of America, American Geophysical Union, and American Association of Geographers national conferences. These results are currently being used as pilot results submitted within a National Science Foundation grant, and will also be presented at the International Association of Geomorphologists conference.

Peyton currently lives in Fort Worth, Texas and is working toward applying for Ph.D. study in fluvial geomorphology at universities in England, Australia, and New Zealand.

ABSTRACT

DISTINGUISHING REACHES IN A TROPICAL HEADWATER STREAM, COSTA RICA: UTILIZING MORPHOLOGY, INSTREAM WOOD, AND TERRESTRIAL LASER SCANNING IN HYDRAULIC CHARACTERIZATION

by Peyton Everett Lisenby, M.S., 2013
Department of Geology
Texas Christian University

Thesis Advisor: Michael Slattery, Professor of Geomorphology,
Director of the Institute of Environmental Studies

Channel morphologies embody the physical reaction between channel substrate, bed material, and flow regime. This study examines reach-scale morphology variability in an ungauged tropical headwater stream. Field morphology classifications are validated through quantifying instream wood distribution and modeling the down-reach hydraulic variation of boundary shear stress and mean stream power. Bifurcated reaches display increased wood abundance and loading, as they provide a means of storage for unattached pieces. This corresponds with the transition from a stepped morphology to a widened, meandering reach that bifurcates around a mid-channel bar, followed by a transition back to a stepped morphology. Hydraulic modeling of two bifurcated reaches demonstrated significant variability in shear stress and stream power in one dimension through these transitions. These results substantiate the effectiveness of coupling field classification schemes with ultra-high resolution topographic surveys when investigating unmonitored streams and they indicate that transitional reaches can punctuate bedform regularity in high-energy drainages.